JOURNAL OF VIROLOGY, Jan. 2005, p. 1164–1179 Vol. 79, No. 2
0022-538X/05/$08.00+0 doi:10.1128/JVI.79.2.1164–1179.2005
Copyright © 2005, American Society for Microbiology. All Rights Reserved.

Mass Spectroscopic Characterization of the Coronavirus Infectious Bronchitis Virus Nucleoprotein and Elucidation of the Role of Phosphorylation in RNA Binding by Using Surface Plasmon Resonance

Hongying Chen,[1] Andrew Gill,[2] Brian K. Dove,[3] Stevan R. Emmett,[3] C. Fred Kemp,[1] Mark A. Ritchie,[2,4] Michael Dee,[2] and Julian A. Hiscox[3,5]*

School of Animal and Microbial Sciences, University of Reading, Reading,[1] Division of Molecular Biology, Institute for Animal Health, Compton,[2] Molecular and Cellular Biology Research Group, Faculty of Biological Sciences,[3] and Astbury Centre for Structural Molecular Biology,[5] University of Leeds, Leeds, and Waters Corporation, Micromass MS Technologies Centre, Wythenshawe, Manchester,[4] United Kingdom

Received 3 September 2003/Accepted 5 July 2004

Phosphorylation of the coronavirus nucleoprotein (N protein) has been predicted to play a role in RNA binding. To investigate this hypothesis, we examined the kinetics of RNA binding between nonphosphorylated and phosphorylated infectious bronchitis virus N protein with nonviral and viral RNA by surface plasmon resonance (Biacore). Mass spectroscopic analysis of N protein identified phosphorylation sites that were proximal to RNA binding domains. Kinetic analysis, by surface plasmon resonance, indicated that nonphosphorylated N protein bound with the same affinity to viral RNA as phosphorylated N protein. However, phosphorylated N protein bound to viral RNA with a higher binding affinity than nonviral RNA, suggesting that phosphorylation of N protein determined the recognition of virus RNA. The data also indicated that a known N protein binding site (involved in transcriptional regulation) consisting of a conserved core sequence present near the 5′ end of the genome (in the leader sequence) functioned by promoting high association rates of N protein binding. Further analysis of the leader sequence indicated that the core element was not the only binding site for N protein and that other regions functioned to promote high-affinity binding.

Avian infectious bronchitis virus (IBV) is a member of the *Coronaviridae* (order *Nidovirales*) (9), members of which are enveloped viruses with single-stranded, positive-sense RNA genomes that are 5′ capped and 3′ polyadenylated (30, 63). The 5′ two-thirds of the coronavirus genome encodes the replicase gene producing two polyproteins, Rep1a and Rep1ab, the latter resulting from a −1 frameshift (7). The remaining proteins, which include the nucleoprotein (N), are expressed from a nested set of subgenomic mRNAs (sgRNAs) that are produced via a discontinuous transcription mechanism (6, 30). Each of these sgRNAs has a short nontranslated leader sequence (64 nucleotides for IBV) derived from the 5′ end of the genome. Present within the leader sequence is a consensus sequence, which we have termed the transcription-associated sequence (TAS) (24). The TAS contains a conserved core motif, which in the case of IBV is CUUAACAA, which is also located in the genome, proximal to the start site for each sgRNA. For different coronaviruses, the core sequence varies and can be present more than once per TAS.

N protein, the virus RNA binding protein, is one of the most abundant viral proteins in an infected cell (31). Several functions have been postulated for the coronavirus N protein throughout the virus life cycle (31); primarily, it complexes with the genomic RNA to form a ribonucleocapsid structure (17) and associates with the M protein (19, 39) to form the viral core (48). While N protein is required in *trans* to rescue the full-length clone of IBV (8) and a porcine coronavirus transmissible gastroenteritis virus clone (82), it is not required for others (1, 71, 72). Certainly, in the case of the rescue of the full-length clone of severe acute respiratory syndrome coronavirus, the presence of N protein increases viral titers compared to rescue performed in the absence of N transcript (83), suggesting that N protein may be involved in the efficiency of replication but that it is not essential.

Based on amino acid sequence comparisons, three domains have been identified in the murine coronavirus, mouse hepatitis virus (MHV) N protein (46), of which the central domain (domain II) was identified as a potential RNA binding site (35, 40) capable of binding both coronavirus- and non-coronavirus-derived RNA sequences (35, 68). However, whether this binding occurs with equal or different affinity is uncertain (14, 35, 49). N protein has been shown to associate with several motifs on viral RNA, including the leader RNA sequence, with particular affinity for the core sequence of the TAS (2, 41), sequences at the 3′ end of the genomic RNA (84), and the packaging signal (37). How these sequences promote N binding is unknown.

Several coronavirus N proteins have been shown to be phosphorylated, including IBV, MHV, and transmissible gastroenteritis virus N proteins, although the precise sites were not identified (31). The role of phosphorylation in the virus life cycle is unknown, although the phosphorylation state of N protein has been predicted to play a role in determining the

* Corresponding author. Mailing address: School of Biochemistry and Microbiology, University of Leeds, Leeds LS2 9JT, United Kingdom. Phone: 44 0113 343 5582. Fax: 44 0113 343 3167. E-mail: j.a.hiscox@leeds.ac.uk.

TABLE 1. Sequences of oligonucleotides used in this study[a]

Oligonucleotide	Sequence (5′–3′)	Polarity
3LeaderTAS	B-ACUUAAGAUAGAUAUUAAUAUAUAUCUAUUACACUAGCCUUGCGCUAGAUUUUUAA**CUGAAC AA**UACAGACCUAAAAAGUCUGUUUGAUG	+
3LeaderSAT	B-ACUUAAGAUAGAUAUUAAUAUAUAUCUAUUACACUAGCCUUGCGCUAGAUUUUUAA**gaacucgu** UACAGACCUAAAAAGUCUGUUUGAUG	+
Random90	B-uucaucuucaucacucaaugaaucacuaagaucagucauucauaugugacuaguga**uauaagau**cauucaaaguugauaaauacuguuaua	+
Random90TAS	B-uucaucuucaucacucaaugaaucacuaagaucagucauucauaugugacuaguga**CUGAACAA**cauucaaaguugauaaauacuguuaua	+
DSL1SL2	B-uucaucuucaucacucaaugaaucacuaagACACUAGCCUUGCGCUAGAUUUUUAA**uauaagau**UACAGACCUAA AAAGUCUGUUUGAUG	+
DSL1SL2rand	B-uucaucuucaucacucaaugaaucacuaagACACUAGCCUUGCGCUAGAUUUUUAA**uauaagau**cauucaaaguugauaaaua cuguuaua	+
DSL1SL2TAS	B-uucaucuucaucacucaaugaaucacuaagACACUAGCCUUGCGCUAGAUUUUUAA**CUGAACAA**UACAGACCUA AAAAGUCUGUUUGAUG	+
SL1SL2TASrand	B-ACUUAAGAUAGAUAUUAAUAUAUAUCUAUUACACUAGCCUUGCGCUAGAUUUUUAA**CUGAAC AA**cauucaaaguugauaaauacuguuaua	+
SL1TASrand	B-ACUUAAGAUAGAUAUUAAUAUAUAUCUAUUaucagucauucauaugugacuaguga**CUGAACAA**cauucaaaguug auaauacuguuaua	+
SL1SL2rand	B-ACUUAAGAUAGAUAUUAAUAUAUAUCUAUUACACUAGCCUUGCGCUAGAUUUUUAA**uauaagau** cauucaaaguugauaaauacuguuaua	+
Antileader	B-CAUCAAACAGACUUUUUAGGUCUGUAUUGUUCAGUUAAAAAUCUAGCGCAAGGCUAGUGUA AUAGAUAUAUAUUAAUAUCUAUCUUAAG	−

[a] The biotin moiety is denoted (B-), the authentic IBV gene 3 sequence is in uppercase, the random sequence is in lower case, and the position of the gene 3 TAS/scrambled/inactive TAS is in boldface type. The sequence that corresponds to predicted SL1 is single underlined, and that corresponding to predicted SL2 is double underlined.

affinity of binding of viral RNA (31, 41), and dephosphorylation of MHV N protein by cellular phosphoprotein phosphatase has been suggested to facilitate the infectious process (36). Siddell et al. (64) identified a virion-associated protein kinase activity that could transfer an additional phosphate from ATP to N protein.

We investigated the role of phosphorylation of IBV N protein in RNA binding by using surface plasmon resonance, which has not previously been used to study coronavirus N protein binding kinetics. To model nonphosphorylated and phosphorylated protein, we expressed and purified N protein from *Escherichia coli* and Sf9 cells, respectively. Mass spectroscopic analysis indicated that the sample expressed in Sf9 cells was phosphorylated proximal to RNA binding domains and had a phosphorylation pattern identical to that of N protein expressed in the model cell line for IBV infection. We used either an IBV-defective RNA to model the viral genome or synthetic RNAmers resembling the viral leader sequence as target RNAs. Our results showed that the phosphorylated form of N protein has decreased affinity for random RNA and that multiple high-affinity N protein binding sites were present on leader RNA.

MATERIALS AND METHODS

Biotinylated RNAmers. Biotinylated RNA oligonucleotides used in this study were obtained from Invitrogen and purified by high-pressure liquid chromatography (HPLC). Their sequences are shown in Table 1 and schematically represented in Fig. 1. Biotinylated oligo(dT) was obtained from Promega.

Recombinant plasmids and viruses. To synthesize recombinant IBV N protein from *E. coli*, the IBV (strain Beaudette) N protein gene was cloned into pTriEx1.1 (Novagen), creating pTriExIBVN, as described previously (81). To synthesize recombinant IBV N protein from insect cells (Sf9), IBV N protein was inserted into BacVector 3000 by using pTriExIBVN as a template for homologous recombination, as described previously (81). The vector places a C-terminal His tag on the N protein and has been used to obtain recombinant purified N protein (13). pCD-61 contains the cDNA for CD-61, an RNA which can be rescued by IBV (15, 47). Vero (simian) cells were maintained in Dulbecco modified Eagle medium supplemented with 10% fetal bovine serum. IBV Beaudette strain was grown in 11-day-old embryonated specific-pathogen-free domesticated fowl eggs and harvested from allantoic fluid for 16 h postinfection.

Infection and transfection of Vero cells. Vero cells (seeded at 10^5 in 9.6 cm^2) were either transfected or infected at 70% confluence. Transfections were performed with 2 μg of pCI-Neo-N with 8 μl of Lipofectamine transfection reagent (Invitrogen) and incubated in Opti-MEM serum-free medium (Invitrogen) at 37°C for 4 h. The transfection medium was replaced with 2 ml of supplemented Dulbecco modified Eagle medium and left for an additional 20 h. Vero cells were infected with 1 ml of IBV Beaudette (multiplicity of infection of approximately 1) and incubated for 1 h at 37°C. The initial inoculum was replaced with 1 ml of media and incubated for a further 7 h postinfection.

Preparation of total protein extracts from Vero cells and Western blotting. Vero cells were washed with phosphate-buffered saline, detached by a cell scraper into 1 ml of phosphate-buffered saline, pelleted by centrifugation at 250 × *g* for 5 min before lysis by addition of 200 μl of cell lysis buffer (20 mM Tris-HCl [pH 7.5], 100 mM NaCl, 0.5 mM EDTA, 0.5% NP-40, and complete protease cocktail inhibitor [Roche]) for 10 min at 4°C. Samples were centrifuged at 10,000 × *g* for 5 min at 4°C, and supernatants were transferred into a new Eppendorf tube and stored at −80°C.

Preparation of N protein from *E. coli*, Sf9, and Vero cells. Expression and purification of His-tagged N protein from either *E. coli* or Sf9 cells has been previously described (12, 13). To obtain N protein from mammalian cells, Vero cells were transfected with pTriExIBVN as described previously (13), and purification was identical to that described for N protein from Sf9 cells. Western blotting was performed by using the ECL detection kit (Amersham Pharmacia) according to the manufacturer's instructions. Briefly, each sample (3 μg of total protein as quantified by Bradford assay) was separated on a 10% NuPage Bis-Tris precast polyacrylamide gel (Invitrogen) in morpholinepropanesulfonic acid (MOPS) running buffer. Protein was transferred onto a polyvinylidene difluoride membrane (Invitrogen) in Invitrogen transfer buffer for 1 h at room temperature. The membrane was blocked for 1 h in Tris-buffered saline (TBS) plus 0.05% Tween 20 and 5% milk. Primary rabbit anti-IBV polyclonal sera (a gift from D. Cavanagh, IAH Compton), diluted 1:10,000 in TBS plus 0.05% Tween 20, was incubated with the membrane for 2 h at room temperature to detect IBV N protein. The membrane was washed three times in TBS plus 0.05% Tween, and then the membrane was incubated with secondary goat anti-rabbit immunoglobulin G conjugated to horseradish peroxidase (diluted 1:1,000 in TBS plus 0.05% Tween) for 1 h at room temperature. The membrane was then washed three times, treated with ECL detection reagents (Amersham Pharmacia), and subjected to autoradiography.

Mass spectroscopy. Recombinant IBV N protein (from *E. coli* [$N_{E.\ coli}$] or Sf9 [N_{Sf9}] cells) was dialyzed into digest buffer (100 mM ammonium bicarbonate, 2 M urea [pH 7.8]). Proteins were digested by the addition of approximately 5 to 10% (wt/wt) endoproteinase Glu-C (Sigma). Resulting proteolytic peptides were analyzed by online capillary HPLC-mass spectrometry (MS). Samples were preconcentrated and desalted by use of a self-packed protein trap, followed by separation by use of a 180-μm-inner-diameter capillary column, self-packed with

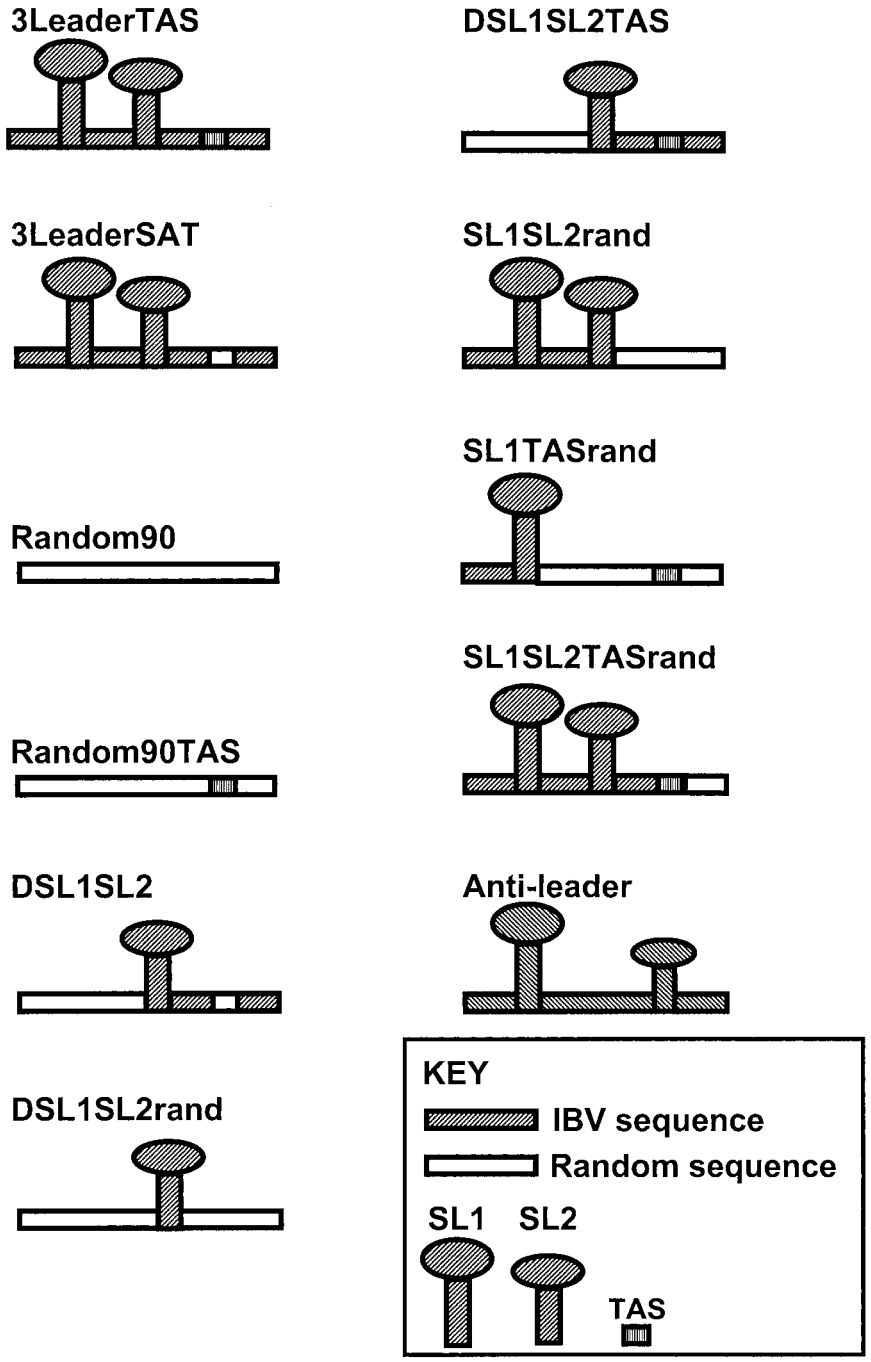

FIG. 1. Diagrammatic representation of the synthetic RNAmers used in this study to show delineation between IBV and a random sequence. Note that SL1 and SL2 are predicted structures only and not yet established by experimental work.

Hichrom C_{18} reversed-phase sorbent (3.5-μm bead size, 150-Å pore size). Peptides were eluted from the column by an increasing gradient of solvent B (0.05% vol/vol trifluoroacetic acid in 5:95 water-acetonitrile), and solvent A was 0.05% vol/vol trifluoroacetic acid in 95:5 water-acetonitrile. The eluent was passed, via a U-Z View UV flow cell (LC Packings), to a Quattro II tandem quadrupole mass spectrometer (Micromass United Kingdom Ltd.). The mass spectrometer was equipped with a commercially available Z-spray source operated in continuous flow nanospray mode. Full-scan mass spectra were acquired in positive-ion mode from an *m/z* of 300 to 2,100 with a scan time of 4 s. The voltage applied to the extraction cone was ramped to improve detection of high-*m/z* ions. Recombinant IBV N protein expressed by Vero cells (N_{Vero}) was digested with trypsin and analyzed by HPLC-MS or automated HPLC-MS/MS at Micromass United Kingdom Ltd. Peptides were separated on a reversed-phase capillary HPLC column (75-μm C_{18} Pepmap; LC Packings), and the eluent was passed directly to the Z-spray source of a Micromass Q-Tof Ultima API (Waters Corp.) mass spectrometer. The mass spectrometer was operated in data-dependent acquisition mode to generate peptide sequence information automatically, and theoretical phosphopeptide ions were added to the include list to ensure that these peptides were sequenced.

Runoff transcription and hybridization of CD-61 RNA to biotinylated oligo(dT). pCD-61 containing the cDNA for the 6.1-kb minigenome of Beaudette IBV was made linear by digestion with NotI. RNA with a 3′ poly(A) tail was in vitro synthesized from pCD-61 by using T7 RNA polymerase (Promega) as described previously (47). RNA (2.5 pmol) was denatured in 400 μl of 0.5 × SSC

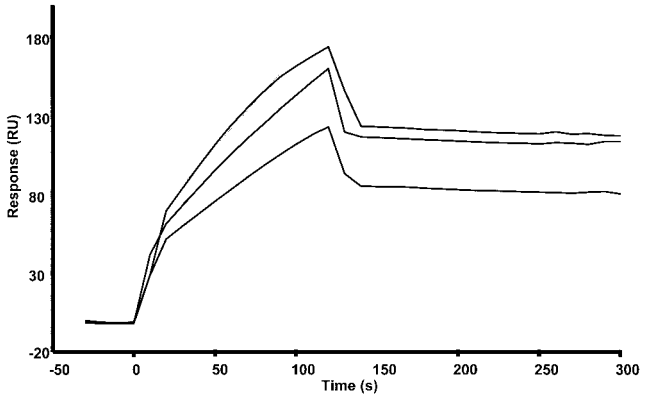

FIG. 2. Sensorgram showing the binding analyte (nonphosphorylated N protein) to target ligand with different flow rates to investigate mass transport effects. N protein (the analyte) at the concentration of 6.25 nM was injected at flow rate of 5, 15, or 75 μl/min. RU, response units.

(1× SSC is 0.15 M NaCl plus 0.015 M sodium citrate) at 65°C for 10 min. Biotinylated oligo(dT) (2.5 pmol) was annealed to the RNA by cooling to room temperature.

Surface plasmon resonance analysis of RNA-protein interactions. Surface plasmon resonance provides both kinetic and equilibrium data about intermolecular interactions and is an excellent tool for the study of RNA-protein interactions (27). In most nucleic acid protein binding studies, RNA is the ligand and is therefore anchored to a solid matrix and the protein is the analyte and is passed over this material (27). In our experiments, kinetic analysis was performed by using a Biacore 3000 (Uppsala, Sweden). Research grade sensor chips coated with streptavidin were obtained from Biacore. Unless otherwise stated, the the running buffer (also used for analyte dilution) was HBS-EP (0.01 M HEPES, 0.15 M NaCl, 3 mM EDTA, 0.005% surfactant P20 [pH 7.4]).

To reduce effects attributed to mass transport, low levels of ligand (given in relative units [RU]) are immobilized on the solid matrix, coupled with a fast flow rate of analyte (27). For example, Stockley et al. (67), in their study of binding of RNA polymerase to immobilized DNA, suggested that between 200 and 800 RU represented low levels of immobilized ligand, and they used a flow rate of 30 or 40 μl/min. Likewise, Waysbort et al. (76) immobilized on average 1,000 RU of ligand and used a flow rate of 5 μl/min of analyte in their study of pyrimidine tract binding protein. Blaesing et al. (4) immobilized between 100 and 700 RU of an oligonucleotide containing a DnaA box motif and a flow rate of 100 μl/min in an investigation of the DNA-binding domain of *E. coli* DnaA protein. In contrast, Park et al. (45) immobilized 30 to 50 RU of target RNA and used a flow rate of 30 μl/min. In a binding study, Kortt et al. (28) found that, with 1,260 or fewer RU of ligand and a flow rate of analyte between 20 and 50 μl/min, no mass transport was apparent and experimental data exhibited no marked deviation from the 1.1 Langmuir binding model used in the study. Given the apparent variation in RU of immobilized ligand used in different binding studies, the average RU of immobilized ligand in our study was approximately 500 RU (as recommended by BIAcoreAB, application note 301, Bianote). The average for CD-61 RNA was 649 RU. For RNAmers, the averages were 526 RU for 3leaderTAS, 490 RU for 3leaderSAT, 488 RU for random90, 488 RU for random90TAS, 435 RU for SL1SL2TASrand, 418 RU for SL1SL2rand, 514 RU for DSL1SL2TAS, 573 RU for DSL1SL2, 560 RU for DSL1SL2rand, 563 RU for SL1TASrand, 450 RU for antileader, 477 RU for 3leaderTAS, 614 RU for 3leaderSAT, 514 RU for random90, and 620 RU for random90TAS.

Prior to our kinetic analysis, we ran control experiments to assess the influence of mass transport on the ligand-analyte interaction and to investigate the use of high flow rates of analyte (N protein) to reduce possible mass flow effects. In brief, different concentrations of N protein were injected at a flow rate of 5, 15, or 75 μl/min over immobilized RNA. As an example, the average binding kinetics of nonphosphorylated N protein (at a concentration of 6.25 nM) to target RNA are shown in Fig. 2 and kinetic values are given in Table 2. The average K_d values obtained were 13.3, 8.44, and 6.97 nM, respectively, indicating that there was no significant difference between the data from a flow rate of 15 to 75 μl/min. Therefore, in subsequent work to study RNA-N protein interactions, and similar to that used by Park et al. (45), we used a flow rate of 30 μl/min to minimize the influence of mass transport.

CD-61 RNA ligand was immobilized to the streptavidin chip by injection of 25 μl of the RNA hybridized with oligo(dT) at a flow rate of 5 μl/min. The kinetic interactions between CD-61 RNA and the IBV N proteins were analyzed by a 6-min injection of the appropriate analyte concentration followed by a 15-min dissociation period. The immobilized CD-61 RNA surface was regenerated by two 30-μl injections of 2 M NaCl and allowed to stabilize for 3 min before the subsequent analyte injection. For the interaction of N proteins with RNA oligomers, biotinylated RNA was diluted to 50 nM with HBS-EP buffer and then 5 μl of RNA was injected at a flow rate of 5 μl/min. Binding experiments were performed at 37°C. Subsequent data were obtained at a rate of 2 points/s. The response from the blank lane alone was subtracted to correct for refractive index changes due to buffer effects and nonspecific interactions with the dextran matrix and presented as sensorgrams of the actual tracings (RU versus time). For all experiments, the data were analyzed by using BIAEvaluation software (version 3.1; Biacore); a statistically significant fit to the binding data was obtained by nonlinear regression. For data analysis, we used models for separated K_a/K_d, i.e., 1:1 (Langmuir) association and 1:1 (Langmuir) dissociation models. After each binding experiment, we monitored for mass transport effects by using the kinetic analysis available on the Biacore 3000. No mass transport effects were observed under the conditions used. To confirm the 1:1 kinetics, we examined the binding of N protein to target RNA by immobilizing CD-61 RNA, injecting over 6.25 nM N protein for 1, 3, or 20 min, and then examining the dissociation rate, which remained unchanged (Fig. 3), indicating that binding was 1:1 and that no secondary binding occurred.

RESULTS

We wanted to investigate the role of phosphorylation and viral RNA sequences in the binding of the coronavirus N protein to RNA by using surface plasmon resonance. Therefore, a source of both purified nonphosphorylated and phosphorylated N protein was required. Previous studies have successfully used a variety of sources of N protein to study RNA binding, including bacterially expressed N protein (41, 84), in vitro-transcribed and -translated N protein (35, 49) (which in both cases were presumably not phosphorylated), or N protein obtained from infected cell lysates (14) (and thus containing a mixture of nonphosphorylated and phosphorylated viral and cellular proteins). It was previously shown that N protein produced in Vero cells (the model mammalian cell line used to study IBV infection) has identical electrophoretic mobility to that produced in insect (Sf9) cells, both of which had slower mobility than N protein produced in *E. coli* (12), suggesting that N protein synthesized in Vero and Sf9 cells had undergone posttranslational modification. We note that Western blot analysis suggested that N protein produced in Vero cells (by transfecting cells with pTriExIBVN [13], a plasmid which expressed N protein under a PolII promoter) has identical mobility to N protein isolated from Vero cells at 8 h postinfection (i.e., the virus has undergone one infectious round) (Fig. 4).

While it was not possible to purify N protein from virions, by

TABLE 2. Average kinetic values for complexes of analyte (nonphosphorylated N protein) with ligand RNA to investigate the effects of mass transport and the use of different flow rates to reduce this effect

Flow rate of mass transfer control (μl/min)[a]	k_a (1/ms)	k_d (1/s)	K_a (1/M)	K_d (nM)
5	3.51×10^4	4.67×10^{-4}	7.52×10^7	13.3
15	4.15×10^4	3.5×10^{-4}	1.19×10^8	8.44
75	5.46×10^4	3.8×10^{-8}	1.44×10^8	6.97

[a] Chi-square test, 1.98.

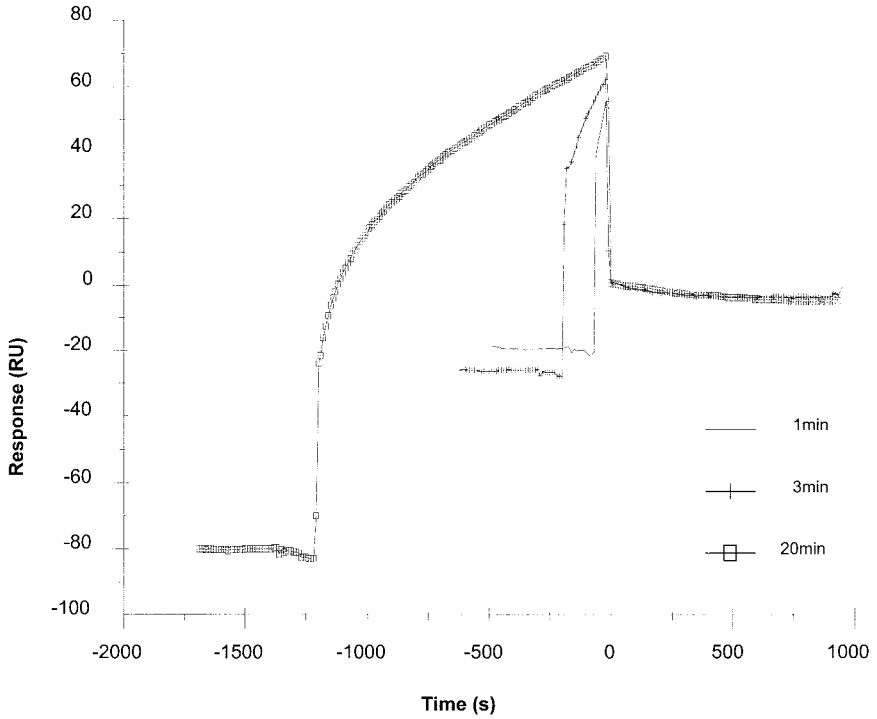

FIG. 3. Sensorgram showing the binding of N protein to CD-61 to investigate whether any secondary binding occurred, 6.25 nM nonphosphorylated N protein was injected for 1, 3, or 20 min. RU, response units.

using mass spectroscopy, we investigated the posttranslational modifications that occurred on N protein produced in Vero cells to N protein produced in Sf9 cells. If posttranslational modifications of N protein in Sf9 cells were the same as N protein synthesized in Vero cells, then we would use N protein produced by the former method as our source of phosphorylated protein for surface plasmon resonance, as larger amounts of protein can be obtained for analysis. N protein produced in and purified from *E. coli*, Sf9 cells, and Vero cells was analyzed by dynamic light scattering (data not shown), which indicated that the protein was monodisperse and had a hydrodynamic radius (whatever the source) of approximately 10 nm.

IBV N protein contains internal disulfide bonds. IBV N protein expressed in *E. coli*, Sf9 cells, and Vero cells was subjected to proteolytic digestion and analysis by capillary HPLC-MS. A representative HPLC chromatogram from analysis of peptides released by tryptic digestion of $N_{E.\ coli}$ is shown in Fig. 5. Many proteolytic peptides were identified, which covered a large amount of the IBV-N protein sequence; peaks are labeled with the residue numbers that the peptides span.

Comparison of peptide profiles before and after reduction with dithiothreitol allowed us to identify various peptides that contained disulfide bonds. Based on the masses of these peptides, we tentatively assigned disulfide bonds between residues Cys281 to Cys308 and Cys320 to Cys323. To confirm these assignments, we also desalted a portion of the peptide mixture by use of a ZipTip and subjected these peptides to tandem MS analysis by using collision activation. Figure 6 shows the tandem mass spectrum of the peptide believed to contain residues 318 to 331, with an internal disulfide bond between residues Cys320 and Cys323. The fragment ions are labeled according to the convention of Roepstorff and Fohlman (50), and this spectrum confirms the identity of the peptide. After reduction, the mass of this peptide increased by 2 Da, and this confirmed the presence of the disulfide bond. Likewise, we obtained MS/MS data that confirmed our assignment of the disulfide bond between Cys281 and Cys308 (data not shown). The presence of these two disulfide bonds was also confirmed in N_{Sf9} by similar methods (data not shown). A range of peptides covering over 65% of the sequence of $N_{E.\ coli}$ was identified, but we found no

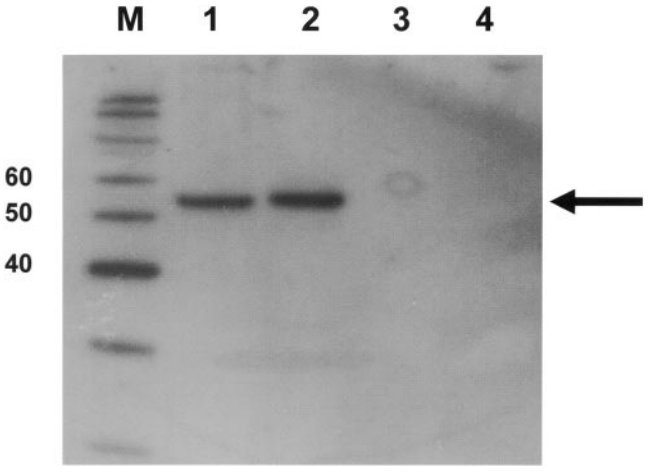

FIG. 4. Western blot analysis of IBV N protein in infected cells (lane 1), cells transfected with a plasmid expressing N protein (lane 2), mock-infected cells (lane 3), and mock-transfected cells (lane 4). The appropriate molecular weight markers are indicated to the left of their lane (M). The position of the IBV N protein is indicated by an arrow.

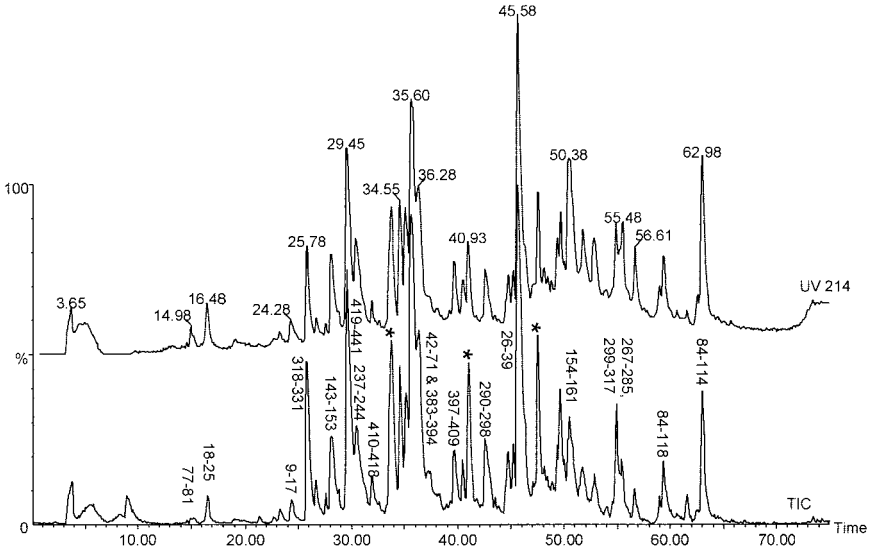

FIG. 5. Capillary HPLC-MS analysis of peptides released after tryptic digestion of $N_{E.\ coli}$. Peptides were detected by both UV absorbance at 214 nm (upper trace) and mass spectrometric total ion current (TIC, lower trace). Peaks in the upper trace are labeled with the retention time of the peptides, and those in the lower trace are labeled according to the residue numbers of $N_{E.\ coli}$ tryptic peptides that were identified. Peaks marked with asterisks correspond to trypsin autolysis products.

evidence for further posttranslational modifications in this protein.

N_{Sf9} contains additional posttranslational modifications. Comparison of digests of $N_{E.\ coli}$ with N_{Sf9} allowed us to investigate posttranslational modifications that are specific to N_{Sf9}. Partial digestion of $N_{E.\ coli}$ with endoproteinase Glu-C produced two N-terminal fragments corresponding to residues 1 to 182 and 1 to 220, which had measured masses close to their theoretical masses, implying that no modifications had occurred within this region (Fig. 7a). The corresponding polypeptides from N_{Sf9} had measured masses that were different from those predicted from the sequence. The measured mass of residues 1 to 182 was 19,574 Da, around 44 Da higher than the measured mass of $N_{E.\ coli}$ protein residues 1 to 182. In addition, N_{Sf9} protein residues 1 to 220 were present in three different forms; the lowest-mass form had a measured mass that was, again, 44 Da higher than that of $N_{E.\ coli}$ residues 1 to 220. The other species had measured masses that were a further 81 and 157 Da higher (Fig. 7b). These mass shifts occurred in the polypeptide spanning residues 1 to 220 but not residues 1 to 182, suggesting that the modifications were within residues 183 to 220.

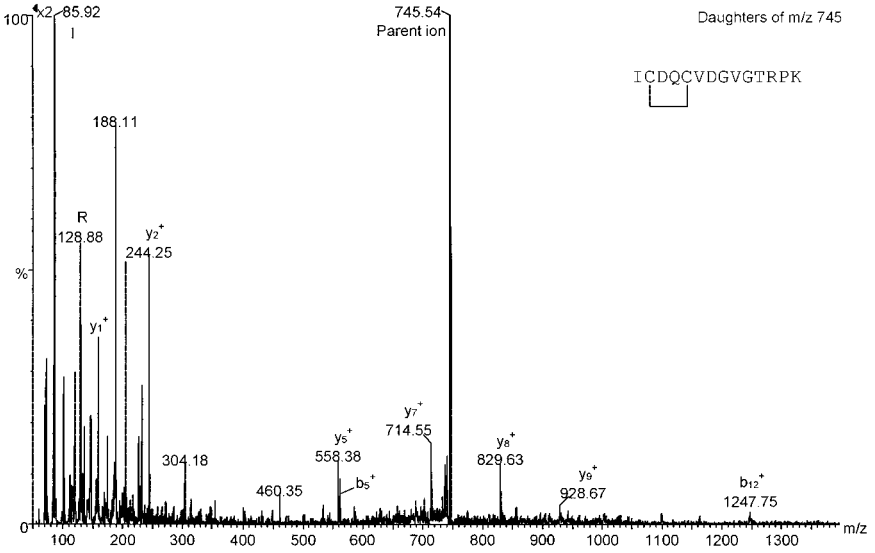

FIG. 6. Tandem mass spectrum of a putative disulfide bond-containing peptide. The peptide covers residues Ile318 to Lys331 and was released by tryptic digestion of $N_{E.\ coli}$. The presence of both diagnostic b and y series fragment ions confirm the identity of this peptide. The mass of the peptide was observed to increase by 2 Da after reduction of disulfide bonds with dithiothreitol, confirming the existence of the single disulfide bond within this peptide.

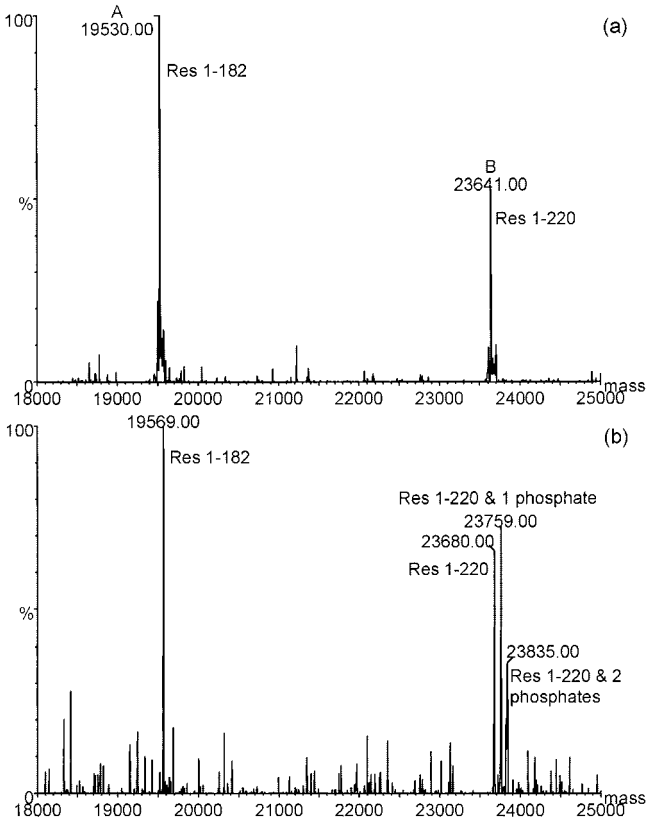

FIG. 7. Deconvoluted electrospray mass spectra of polypeptides released by endoproteinase Glu-C digestion of $N_{E.\ coli}$ (a) and N_{Sf9} (b) proteins. (a) Peaks corresponding to residues 1 to 182 (theoretical mass, 19,531.7 Da) and 1 to 220 (theoretical mass, 23,641.3 Da) are evident. (b) Peaks corresponding to the same polypeptides have masses that have increased by around 40 Da. This mass difference was measured to be 44 Da from the original peak envelopes. In addition, the polypeptide spanning residues 1 to 220 is present in three different forms, with each separated by around 80 Da. This is consistent with up to two phosphorylations in this polypeptide. The absence of these signals in the peptide corresponding to residues 1 to 182 implies that the sites of phosphorylation are between residues 183 and 220.

The modification of 44 Da within residues 1 to 182 was consistent with acetylation (addition of 42 Da), and a proteolytic peptide spanning residues 1 to 51 also carried this modification (measured difference, 42.6 Da) (data not shown). The measured mass differences occurring between residues 183 to 220 were consistent with the addition of two phosphate groups (phosphorylation results in a mass increase of 80 Da per group). Endoproteinase Glu-C digestion also generated C-terminal peptides with different masses between $N_{E.\ coli}$ and N_{Sf9} proteins, suggesting additional phosphorylation sites within this domain (data not shown).

Residues in both the N- and C-terminal domains are phosphorylated in both N_{Sf9} and N_{Vero}. To locate the sites of phosphorylation, N_{Sf9} was digested with trypsin to yield smaller fragments; the peptide pool was desalted by use of a ZipTip and was analyzed by offline MS in negative-ion mode. To specifically detect phosphopeptides, a precursor ion scan was used that detected peptides fragmenting to yield a moiety of an *m/z* of 79 (PO_3^-). The resulting spectrum is shown in Fig. 8, and peaks are labeled with putative residue numbers of the peptides, assigned solely from the peptide mass. From these data, it appears that there are two sites of phosphorylation between residues 186 to 198 and a further two between residues 367 to 394. A fresh aliquot of tryptic peptide mixture was analyzed in positive-ion mode, and the relevant phosphopeptides were subjected to collision activation experiments by MS/MS. The MS/MS spectrum of the doubly phosphorylated peptide with a mass of 3,460.4 Da from N_{Sf9} is shown in Fig. 9a. Fragment ions are labeled according to the convention of Roepstorff and Fohlman (50). Neutral losses of 98 Da (H_2PO_4) from the parent ion, characteristic of phosphopeptides, was observed. In addition, structural information was obtained from sequence-specific fragment ions, which are shown more clearly in the magnified inset of Fig. 9a. By comparison with corresponding MS/MS spectra of singly and unphosphorylated peptides, the sites of phosphorylation were distinguished. The data showed that the peptide spans residues 367 to 394 and that the sites of phosphorylation are Thr378 and Ser379. In the singly phosphorylated peptide, however, it is not clear which of these two sites is occupied.

MS/MS spectra were also obtained on putative phosphopeptides from the N-terminal region of N_{Sf9} (data not shown), and these confirmed that the sites of phosphorylation are Ser190 and Ser192. The MS/MS spectrum of the nonphosphorylated peptide confirmed the identity of the peptide, whereas that of the singly phosphorylated peptide demonstrated that Ser192 was occupied in preference to Ser190.

To confirm that these phosphorylation sites were present in N protein expressed by mammalian cells, the protein was expressed in Vero cells (N_{Vero}), digested with trypsin, and analyzed by HPLC-MS. Since the amount of protein obtained from these cells was low, this analysis was performed by use of a more-sensitive mass spectrometer, a Q-ToF instrument. The tryptic digest of N_{Vero} was similar to that of N_{Sf9}, and putative phosphopeptides were observed with the same masses as measured for N_{Sf9}. Operating in data-dependent acquisition mode allowed peptides to be automatically subjected to MS/MS analysis as they eluted from the column, and this included putative phosphopeptides. The MS/MS spectrum of the singly phosphorylated peptide spanning residues 188 to 198 from N_{Vero} is shown in Fig. 9b. It is identical to that obtained from N_{Sf9} (data not shown) and confirms that the initial site of phosphorylation in the N-terminal region is Ser192. We also obtained MS/MS spectra for the C-terminal phosphorylation sites. Our data indicated that the same phosphorylation sites were occupied in N_{Vero} as were found in N_{Sf9}, establishing that N_{Sf9} is a relevant model for phosphorylated N protein and thus could be used for kinetic analysis. N protein produced in *E. coli* is subsequently referred to as $N_{nonphos}$, and N protein produced in Sf9 cells is referred to as N_{phos}.

Comparison of the affinity of binding of nonphosphorylated and phosphorylated forms of N protein with viral RNA by using surface plasmon resonance. We compared the binding of $N_{nonphos}$ protein and N_{phos} protein with two models of the IBV genome. The first was RNA synthesized by in vitro transcription from pCD-61. The second was a synthetic biotinylated RNA, RNAmer 3LeaderTAS, which was identical to the 5′ end of IBV mRNA 3 up to, and including, the translation initiation codon for gene 3a. CD-61 RNA was generated by

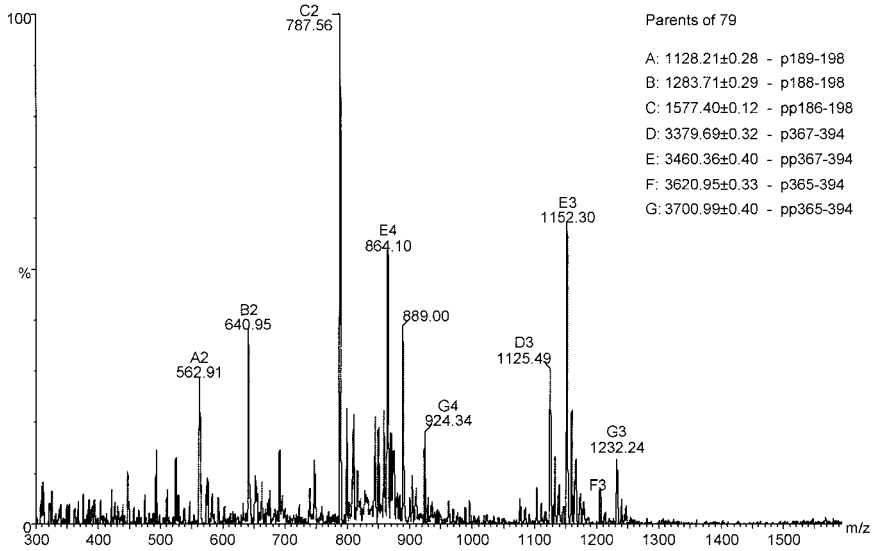

FIG. 8. Negative-ion mass spectrometric analysis of tryptic peptides of N_{Sf9} by offline precursor ion scanning. The mass spectrum shows all ions that fragment to give a specific fragment ion with an *m/z* of 79 (PO_3^-). Peaks are labeled with a letter to identify the peptide and a number corresponding to the charge state. Although many signals are evident, this is the result of heterogeneity in digestion and phosphorylation. All peptides span essentially the same residues in the N- and C-terminal domains, and these data suggest up to two phosphorylations between residues 186 and 198 and an additional two between residues 367 and 394.

runoff transcription from pCD-61 and hybridized to oligo(dT), which was immobilized on a streptavidin flow cell.

Various concentrations of either $N_{nonphos}$ or N_{phos} proteins were passed over immobilized CD-61 RNA. The resultant sensorgrams are shown in Fig. 10, and kinetic analysis is shown in Table 3. The data suggested that there was no significant difference in the binding of $N_{nonphos}$ protein (K_d, 8.89 ± −0.08 nM) to CD-61 than N_{phos} protein (K_d, 16.9 ± −0.53 nM), which indicated that both forms of N protein associated with viral RNA with high affinity. The preparation of the CD-61–oligo(dT) complex may also have contained free oligo(dT), which was available to bind to the streptavidin flow cell. However, we found that N protein did not bind to immobilized oligo(dT) (data not shown), suggesting that any binding characteristics of the CD-61–oligo(dT) complex were due to interactions with CD-61 RNA only.

Biotinylated RNAmer 3LeaderTAS was immobilized directly onto the streptavidin flow cell, 12.5 nM $N_{nonphos}$ protein or N_{phos} protein was passed over, and the binding affinity was determined. The sensorgrams for 3LeaderTAS with N_{phos} and $N_{nonphos}$ proteins are shown in Fig. 11 and 12, respectively. The kinetic analysis of the binding experiments is shown in Table 4. On first inspection, the data indicated that $N_{nonphos}$ protein (K_d, 0.657 nM) had a higher affinity for 3LeaderTAS than N_{phos} protein (K_d, 2.82 nM). However, we found that the variation in binding affinities between replicate experiments with RNAmers was approximately ±1.5 nM (data not shown), and therefore, the binding of $N_{nonphos}$ protein and N_{phos} protein with 3LeaderTAS was not significantly different. Although these binding affinities were higher than with CD-61, they both reflected high-affinity binding of N protein with viral RNA.

Phosphorylation decreases the affinity of N protein for random RNA. As a model for nonviral RNA, we synthesized a biotinylated RNAmer (Random90) of identical length to RNAmer 3LeaderTAS that was based on the *E. coli* sequence, but the GC content was reduced to reflect a GC ratio (28%) similar to that of the leader RNA. The biotinylated RNAmer was immobilized to the streptavidin flow cell, and then 12.5 nM concentrations of both forms of N protein were injected for 360 s. The sensorgrams for RNAmer Random90 are shown in Fig. 11 and 12. The kinetic analysis of the binding experiments is shown in Table 4. The binding affinity of N_{phos} protein to RNAmer Random90 was 810 nM compared to 3.24 nM for $N_{nonphos}$ protein, a 250-fold difference. This was probably because the association rate of N_{phos} protein to RNAmer Random90 is approximately 170 times lower than that of $N_{nonphos}$ protein. The dissociation rates for both proteins are approximately the same. These data indicate that phosphorylation of N protein decreases the affinity for random RNA. A side-by-side comparison of the binding of both species of N protein with 3LeaderTAS and Random90 is also shown in Fig. 12.

Core sequence determines association rate. We investigated the effect of the core sequence on RNA binding by using two different approaches: by scrambling the core sequence from gene 3 (RNAmer 3LeaderSAT) and by replacing eight nucleotides of the Random90 sequence with the gene 3 core site (RNAmer Random90TAS) in the same location as the viral RNA, i.e., at nucleotide 57 of the leader sequence. The mutations introduced into the gene 3 core sequences in RNAmer 3LeaderSAT were the same mutations that abolished transcription in an IBV minireplicon (65) and were thus biologically relevant. Both biotinylated RNAmers were immobilized to the streptavidin flow cell, and then 12.5 nM N_{phos} protein was passed over these ligands for 360 s. The sensorgrams for 3LeaderSAT and Random90TAS are shown in Fig. 11. The kinetic analysis of the binding experiments is shown in Table 4. Abolition of the core sequence did not appear to significantly affect the affinity of binding of N_{phos} to the IBV gene 3 leader sequence. However, the addition of the core site to Random90

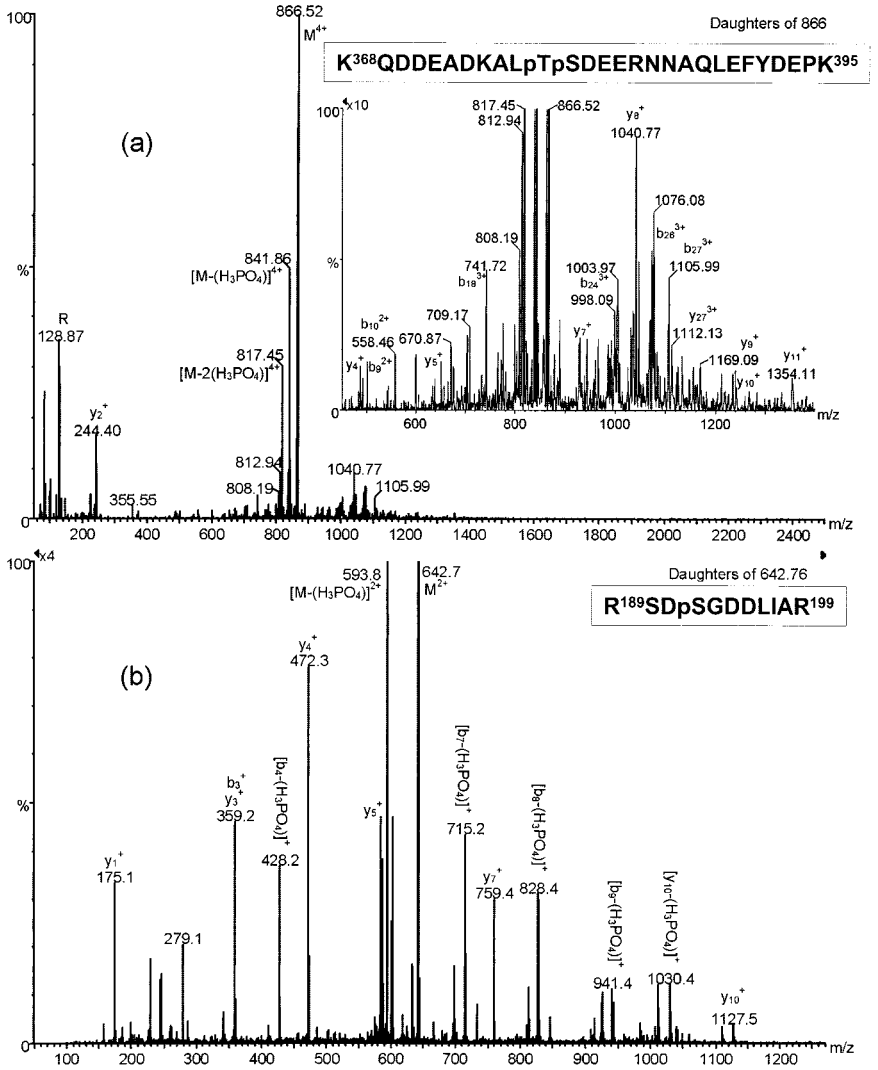

FIG. 9. Tandem mass spectra of phosphopeptides released after tryptic digestion of N_{Sf9} (a) and N_{Vero} (b). The parent ion in panel a had an *m/z* of 866, corresponding to the putative diphosphorylated peptide of residues 367 to 394 with four charges. Characteristic neutral losses of 98 Da, *m/z* of 841.86 and 817.45, can be observed. The inset in panel a is a magnification of the region of the spectrum containing sequence-specific fragment ions and confirms the identity of the peptide and the sites of phosphorylation as Thr378 and Ser379. The parent ion in panel b had an *m/z* of 642.8, corresponding to the peptide of residues 188 to 198 with a single phosphorylation. A single neutral loss to an *m/z* of 593.8 is evident. The sequence-specific fragment ions confirm the identity of the peptide and conclusively indicate the site of phosphorylation as Ser190. In all cases, peaks are labeled according to the fragment ion nomenclature of Roepstorff and Fohlman (50).

increased the affinity of binding of N_{phos} protein to RNA approximately 240 times, mainly due to the increased association rate, indicating that the core site affected the association rate between N_{phos} protein and RNA but not the dissociation rate. The same trend was observed for the binding of $N_{nonphos}$ protein to these RNAmers (Table 4; Fig. 11), and the difference in binding affinity by $N_{nonphos}$ protein and the different RNAmers was less than that for the N_{phos} protein.

Multiple N protein binding sites are present in leader sequence. The above data indicated that, although the TAS acted to promote high-affinity binding of N protein on a nonviral RNA, when the site was mutated in the leader sequence, there was no significant difference to binding, suggesting that other binding sites may be present. Analysis of the structure of the IBV leader sequence indicated that two predicted stem-loops were formed and that the sequences corresponding to these predicted structures were conserved in different strains (66). Where nucleotide differences occurred between strains, a corresponding covariant mutation was present to conserve the appropriate predicted stem-loop structure (66). Predicted stem-loop one (SL1) is formed between nucleotides 7 and 30, and predicted stem-loop two (SL2) is formed between nucleotides 34 and 48. Although a third stem-loop is formed when predicting the structure of the leader sequence, this feature is not present when the analysis is extended in the 3′ direction (P. Britton, personal communication). Therefore, we investigated the role of the two conserved predicted stem-loop regions upstream of the core element in binding phosphorylated N protein. Appropriate regions of the leader sequence were replaced with the corresponding nucleotides from the random nonviral

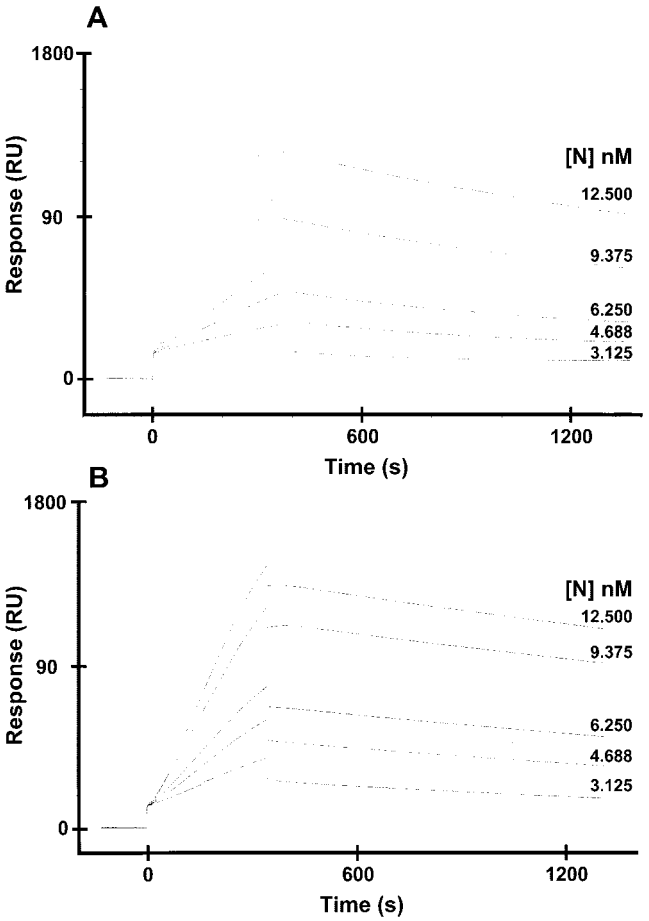

FIG. 10. Sensorgrams showing the binding of different concentrations (indicated above the appropriate nanomolar concentration) of either phosphorylated (A) or nonphosphorylated (B) N protein to CD-61 RNA by using surface plasmon resonance. RU, response units.

RNA. All subsequent experiments were conducted with N_{phos} protein, as this protein could distinguish between nonviral and viral RNA and probably represents the predominant form of N protein in the infected cell and virion (31).

Replacement of sequence downstream of the TAS with random RNA (RNAmer SL1SL2TASrand) did not affect the binding affinity of N protein when compared to 3LeaderTAS (K_d, 2.59 and 2.82, respectively) (Table 4; Fig. 11). The association rate was three times slower. The binding affinity of N_{phos} protein on SL1SL2rand was also less (K_d, 11.7) when compared to SL1SL2TASrand (K_d, 2.59), which is a reflection of the lower association rate, again indicating that the TAS contributes to association rate (e.g., Random90TAS has the fastest association rate for the binding of N_{phos} protein).

SL2 can act as a high-affinity N protein binding site. Replacement of SL1 with random RNA (RNAmer DSL1SL2TAS) did not appear to significantly affect the binding affinity (K_d, 2.42) when compared to the leader RNA (K_d, 2.82), although the disassociation rate was slower (Table 4; Fig. 11). The association rate of N_{phos} protein with RNA was lower with DSL1SL2 compared to the leader RNA, and the binding affinity was approximately five times less. Interestingly, the data indicated that SL2 by itself could act as a high-affinity binding region for N protein, as replacement of flanking sequences with random RNA gave a binding affinity with a K_d of 1.51.

Role of SL1 in N protein binding. SL2 and sequences downstream of the TAS were replaced with random RNA, forming RNAmer SL1TASrand, so the RNA contained only SL1 and a TAS. N_{phos} protein bound to this RNA with higher affinity (K_d, 0.63) than to the leader RNA (Table 4; Fig. 11). Unfortunately, an RNAmer containing SL1 only proved difficult to synthesize, and thus, we were unable to determine the binding affinity of N_{phos} protein to SL1. However, the binding affinity of N_{phos} protein to SL1TASrand is greater than to RandomTAS, suggesting that SL1 can promote high-affinity binding.

Binding of N_{phos} protein to antileader RNA. In coronavirus-infected cells, negative-sense copies of sgRNAs are present and contain antileaders (60). These negative-strand RNAs can act as templates for the synthesis of positive-strand sgRNAs (24, 54–57, 59). We investigated the binding of N_{phos} protein to antileader RNA. This RNAmer was the exact anticopy of 3LeaderTAS, except that it was one nucleotide shorter because the synthesis process could not terminate with a U (Invitrogen). The kinetic analysis (Table 4; Fig. 11) indicated that N_{phos} protein formed a high-affinity association with antileader (2.17 nM).

DISCUSSION

The RNA binding kinetics of the coronavirus nucleoprotein to RNA and relevant binding motif(s) and the role of phosphorylation in this process has not previously been determined. To model this, we made use of IBV N protein purified from either *E. coli* or Sf9 cells to generate nonphosphorylated and phosphorylated proteins, respectively, which we have used to study interactions with nucleolin (13). Mass spectroscopy confirmed that N protein purified from *E. coli* was nonphosphorylated, whereas N protein purified from Sf9 cells was phosphorylated. These phosphorylation sites were identical to the phosphorylation sites found on N protein expressed in Vero cells, which is the mammalian cell line model for IBV. The data suggested that IBV N protein could be phosphorylated at two clusters, amino acid residues Ser190 and Ser192 and Thr378 and Ser379, which are proximal to RNA binding domains. The majority of species was either mono- or biphosphorylated. These sites are predicted casein kinase II (CKII)

TABLE 3. Average kinetic values for complexes of phosphorylated and nonphosphorylated N protein with CD-61[a]

Analyte concn (nM)	k_a (1/ms)	k_d (1/s)	K_a (1/M)	K_d (nM)
12.50	3.21×10^4	3.25×10^{-4}	9.89×10^7	10.10
	3.45×10^4	2.1×10^{-4}	1.64×10^8	6.08
9.375	2.04×10^4	3.74×10^{-4}	5.46×10^7	18.30
	4.31×10^4	2.22×10^{-4}	1.94×10^8	5.16
6.25	1.78×10^4	4.49×10^{-4}	3.96×10^7	25.30
	4.26×10^4	2.86×10^{-4}	1.49×10^8	6.72
4.69	2.44×10^4	4.72×10^{-4}	5.16×10^7	19.40
	3.34×10^4	3.4×10^{-4}	9.81×10^7	10.20
3.13	3.19×10^4	3.71×10^{-4}	8.61×10^7	11.60
	2.82×10^4	4.61×10^{-4}	6.12×10^7	16.30

[a] For each analyte concentration, the result for phosphorylated N protein is given above the result for nonphosphorylated N protein.

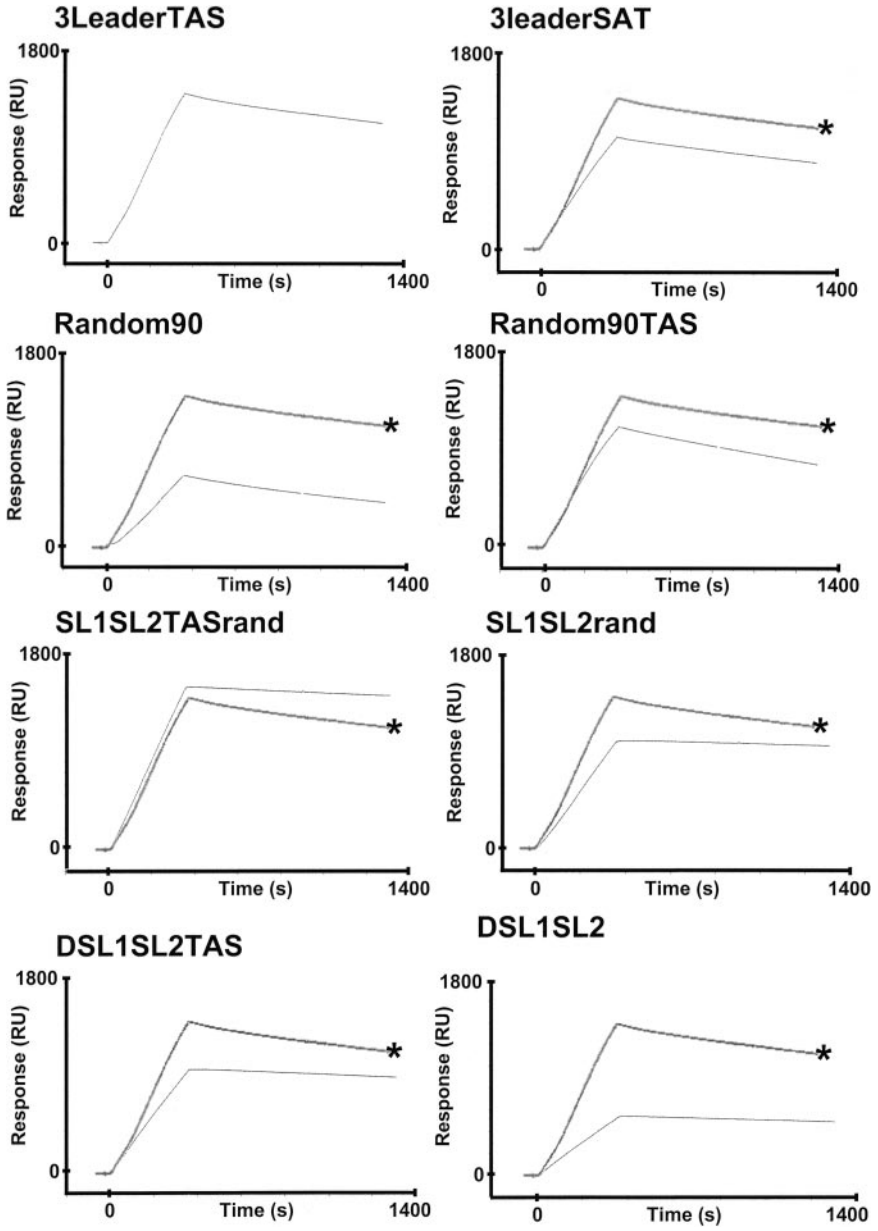

FIG. 11. Sensorgrams showing the binding of phosphorylated N protein to various biotinylated RNAmers (indicated) by using surface plasmon resonance. RU, response units. The sensorgram for 3LeaderTAS (indicated by an asterisk) is superimposed for reference.

phosphorylation sites (32). Additional acidic amino acids in positions +1, +2, +4, and +5 have been reported to increase the phosphorylation rate at CKII sites, whereas a basic residue N-terminal of the site will decrease the phosphorylation rate. In the case of Ser190, there are acidic amino acids in the +1 (Asp191), +4 (Asp193), and +5 (Asp194) positions (Fig. 13). However, there are two basic residues N-terminal of this site (Arg188 and Arg189), which may account for the observation that Ser192 was occupied in preference to Ser190. In the case of Ser192, there are acidic amino acids in the +2 (Asp193) and +3 (Asp194) positions (Fig. 13). For the C-terminal phosphorylation sites, Thr378 has preferential acidic amino acids in the +2 (Asp380) and +4 positions (Asp382) and Ser379 has preferential acidic amino acids in the +1 (Asp380) and +2 (Asp381) positions (Fig. 13). CKII is present in the mitochondria and cytoplasm, but predominately in the nucleus, and several nuclear proteins serve as substrates, for example, p53, RNA polymerases I and II, and the nucleolar proteins B23 and C23 (32). Phosphorylation by CKII alters the nucleic acid or catalytic activity of some of these substrates. Coronavirus N proteins have both a cytoplasmic and nuclear/nucleolar distribution (25, 42, 81), as do other N proteins of the *Nidovirales* (51, 52, 74). Therefore, it is interesting to speculate that coronavirus N proteins can be posttranslationally modified by nuclear proteins (e.g., phosphorylation by CKII), suggesting nuclear involvement in positive-strand RNA virus replication (22, 23, 77). CKII has also been shown to be involved in the phosphorylation and transcriptional activity of a number

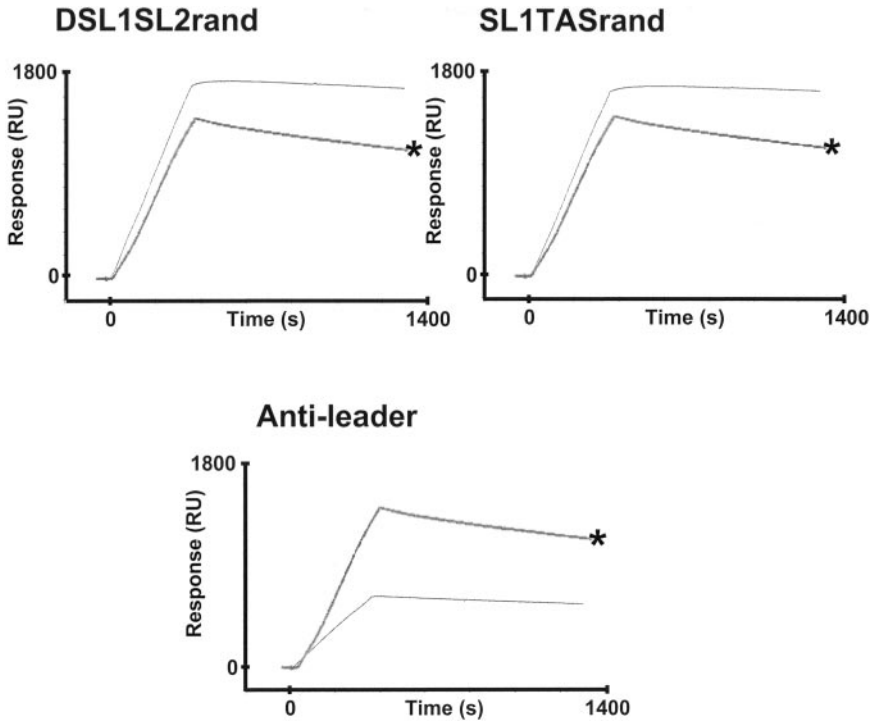

FIG. 11—*Continued.*

of viral proteins, including vesicular stomatitis virus P protein (3).

HPLC analysis of tryptic phosphopeptides revealed that phosphorylation of MHV N protein occurred at only two or three sites (79), which Laude and Masters (31) suggested was relatively small, given that MHV N protein had some 30 to 40 potential target residues for phosphorylation. Sequence analysis indicated that IBV had at least 10 potential residues for phosphorylation (53); however, our mass spectroscopy results for IBV N protein would support the hypothesis that relatively few potential sites of phosphorylation in the coronavirus N proteins are phosphorylated.

Although our principal aim with mass spectroscopy was to investigate the phosphorylation status of N protein, analysis revealed several other potential modifications. We found that the N-terminal region of N protein may be acetylated. Acetylation in the N-terminal region of both cellular and viral proteins is a common posttranslational modification, e.g., the phosphoprotein (P) of some paramyxoviruses (62). Although acetylation of proteins has a number of different functions, it is also involved in transcriptional regulation, e.g., acetylation of human immunodeficiency virus Tat protein (43) and CREB-mediated gene expression (33). Acetylation of the coronavirus N protein could therefore play a role in the transcriptional regulatory activity the protein may display. N protein from the three different sources had identical disulfide bridges, formed between residues Cys281 and Cys308 and Cys320 and Cys323. Analysis of N protein by sodium dodecyl sulfate-polyacrylamide gel electrophoresis analysis under native conditions indicated that the predominant species in solution were both monomeric and multimeric (but not dimeric), whereas under reducing conditions, N protein was present as a monomer only (12). Although these bridges may have formed during the extraction and purification of the protein, normally when this occurs, disulfide bridge formation occurs sequentially, and therefore, we would have predicted that disulfide bridges would form between Cys228 and Cys281 and Cys308 and Cys320. However, we did not observe this. Although N protein is cytosolic, non-endoplasmic reticulum-based redox pathways can contribute to disulfide bridge formation (61). Disulfide bridge formation may therefore be important in the correct folding of N protein. However, it should be noted that the severe acute respiratory syndrome coronavirus N protein does not contain any cysteine residues and therefore would not contain disulfide bridges (34).

Surface plasmon resonance (Biacore) has not previously been applied to the study of the interaction of coronavirus N protein with coronavirus RNA. Therefore, we used this technique to investigate the interaction of nonphosphorylated and phosphorylated IBV N protein with a variety of viral and nonviral target RNAs. In the case of the biotinylated RNAmers, we were able to examine the interaction of N protein with target RNAs at near physiological temperature (37°C). We examined the binding of nonphosphorylated and phosphorylated N protein on both the gene 3 leader sequence and CD-61. There was no significant difference in the binding of nonphosphorylated and phosphorylated N protein to leader RNA or a defective interfering RNA (DI-RNA). Our results are in contrast to those of Cologna et al. (14), who found that the bovine coronavirus (BCoV) N protein bound more efficiently to a BCoV minireplicon than to the BCoV leader sequence. This discrepancy may be due to the differences between filter binding assays used by Cologna et al. (14) and surface plasmon resonance (45) used in our study, or it may be an intrinsic property of the different coronavirus N proteins. However, our results suggested that phosphorylated N protein had 264 times

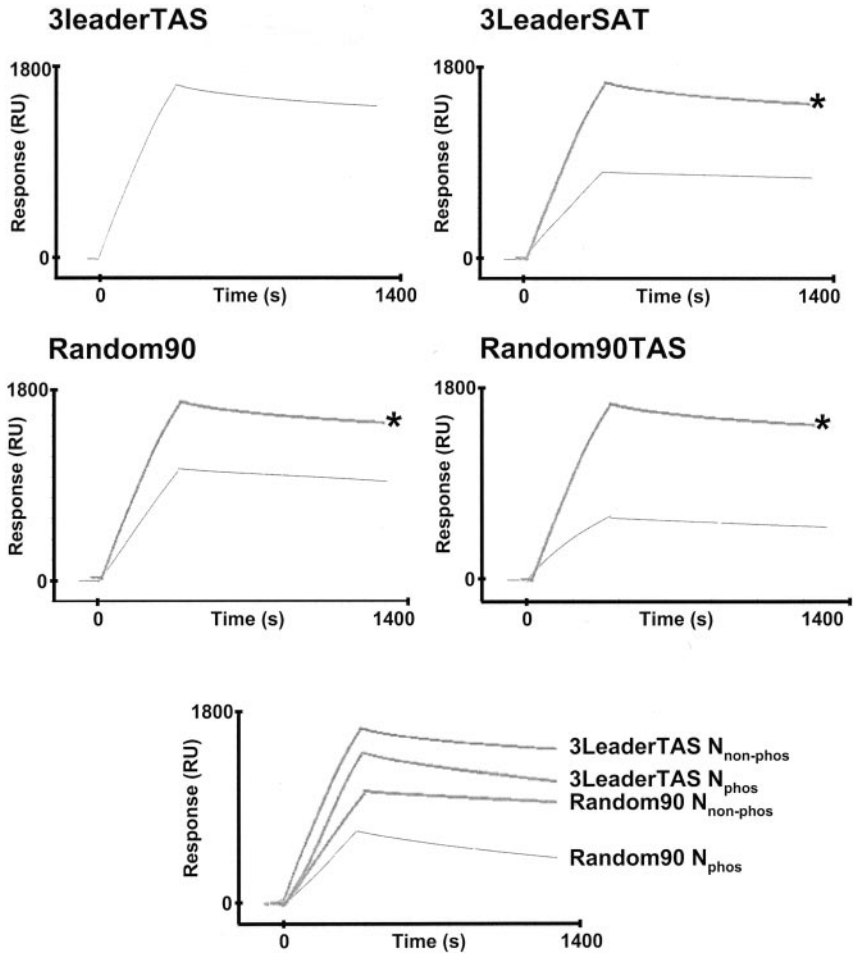

FIG. 12. Sensorgrams showing the binding of nonphosphorylated N protein to various biotinylated RNAmers (indicated) by using surface plasmon resonance. RU, response units. The sensorgram for 3LeaderTAS (indicated by an asterisk) is superimposed for reference. The bottom sensorgram is for comparison of the binding of nonphosphorylated ($N_{nonphos}$) and phosphorylated (N_{phos}) N protein to both 3LeaderTAS and Random90.

greater affinity for the leader sequence than a nonviral RNA. N protein failed to bind to an oligomer with 25 T residues, indicating that sequence context may be important for nucleotide binding. The differences in the amount of N binding to RNA, the source of N protein, and the kinetics of this interaction may account for why previous studies could not resolve whether N bound either specifically to viral RNA or bound with equal affinity to both viral and nonviral RNA.

Nelson et al. (41) measured the binding affinity of MHV N protein (isolated from *E. coli* and therefore nonphosphorylat-

TABLE 4. Average kinetic values for complexes of phosphorylated and nonphosphorylated N protein with target RNAmers[a]

Target RNA	k_a (1/ms)	k_d (1/s)	K_a (1/M)	K_d (nM)
3LeaderTAS	7.81×10^4	2.20×10^{-4}	3.55×10^8	2.82
	1.58×10^5	1.04×10^{-4}	1.52×10^9	0.657
3LeaderSAT	6.38×10^4	2.36×10^{-4}	2.7×10^8	3.70
	4.48×10^4	7.24×10^{-5}	6.19×10^8	1.62
Random90	606	4.9×10^{-4}	1.24×10^6	810
	1.02×10^5	3.30×10^{-4}	3.08×10^8	3.24
Random90TAS	1.12×10^5	3.82×10^{-4}	2.94×10^8	3.40
	1.59×10^5	1.70×10^{-4}	9.34×10^8	1.07
SL1SL2TASrand	2.36×10^4	6.11×10^{-5}	3.86×10^8	2.59
SL1SL2rand	4.73×10^3	5.53×10^{-5}	8.56×10^7	11.7
DSL1SL2TAS	3.83×10^4	9.26×10^{-5}	4.13×10^8	2.42
DSL1SL2	7.41×10^3	1.12×10^{-4}	6.62×10^7	15.10
DSL1SL2rand	2.94×10^4	4.44×10^{-5}	6.61×10^8	1.51
SL1TASrand	4.21×10^4	2.65×10^{-5}	1.59×10^9	0.63
Antileader	5.73×10^4	1.24×10^{-4}	4.62×10^8	2.17

[a] Where two values are given for a target RNA, the result for phosphorylated N protein is given above the result for nonphosphorylated N protein.

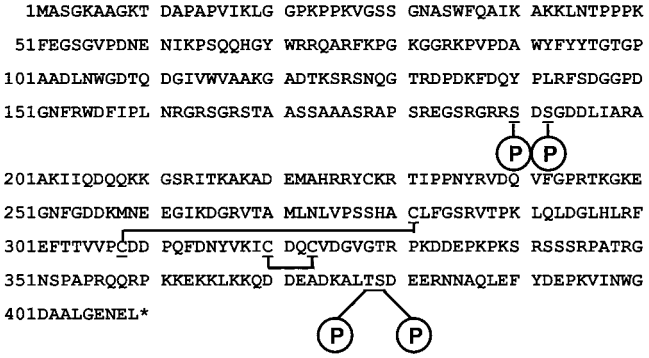

FIG. 13. Amino acid sequence of the IBV Beaudette strain N protein (5) showing the sites of phosphorylation and disulfide bridge formation.

ed) to the MHV leader sequence and obtained a K_d of 14 nM. Although the binding affinity of IBV $N_{nonphos}$ protein to the IBV leader (K_d, 0.66 nM) is greater than that of MHV N protein to MHV leader, this may be a reflection of the differences in recombinant N protein preparation (His tag in the case of IBV N protein versus glutathione *S*-transferase fusion for MHV N protein) and kinetic measurement (surface plasmon resonance versus filter binding assay). With that said, the binding affinity of MHV N protein to MHV leader (41) and IBV N protein to IBV leader is very strong and thus probably reflects a general pattern for coronaviruses. Consideration should be given to the fact that N protein in virions and the infected cell is exclusively phosphorylated and is probably not nonphosphorylated (31). A phosphoamino acid analysis of the arterivirus (a member of the *Nidovirales*) porcine reproductive and respiratory syndrome virus nucleocapsid protein revealed that this protein was also exclusively phosphorylated, and no nonphosphorylated species were found (80). Therefore, care should be taken when interpreting the results obtained with nonphosphorylated N protein and drawing biologically relevant conclusions, as this form of N protein is probably not present in virus-infected cells. We favor the hypothesis that the role of phosphorylation is to decrease the affinity of N protein for random RNA so that N protein associates with viral RNA in preference to cellular RNA.

Comparison of the binding affinity between IBV N protein and RNA and other RNA binding proteins also revealed that N protein had high-affinity binding. Using surface plasmon resonance, Park et al. (45) determined the binding affinity for human neuron-specific RNA binding (HuD) protein with AU-rich target biotinylated RNAs was approximately 0.7 nM. In this experiment, recombinant HuD protein was C-terminally His tagged and purified from *E. coli* and presumably nonphosphorylated. The binding affinity of IBV $N_{nonphos}$ and N_{phos} protein to leader RNA is similar.

The principal function of N protein in terms of the infectious cycle of the virus can perhaps be viewed as binding to viral RNA to form the ribonucleocapsid structure, part of the core particle. In a number of viruses, viral capsids can form in the absence of RNA and instead can be replaced with either cellular RNAs or suitable polyanions; this has been perhaps best characterized in the encapsidation and assembly of nodavirus particles (29, 58, 73). The high affinity of phosphorylated N protein for viral RNA over nonviral RNA together with appropriate packaging signals (16, 18, 20, 37) may explain why virions are composed of viral RNA (48).

Using the phosphorylated form of N protein, we found that the IBV gene 3 core sequence contributed to the kinetics of RNA binding. Introducing a core sequence into nonviral RNA (Random90) increased N binding, with the major change being in the association rate. Scrambling the core sequence in the context of the leader RNA resulted in only a small decrease in binding affinity, suggesting that the core sequence was not the only N protein-binding site present on leader RNA. Stirrups et al. (66) described two conserved predicted stem-loops that were present upstream of the core sequence in the leader sequence. By replacing these sequences with random RNA (from Random90), that did not promote high-affinity binding, we showed that the sequences that form predicted SL1 and predicted SL2 both contributed to high-affinity binding of phosphorylated N protein to leader RNA. However, it should be noted that optimum RNA ligand binding sequences are not necessarily the same as those found in vivo (78). The high-affinity binding of N protein to the stem-loop structures may suggest that N protein could be a general double-stranded RNA binding protein. However, structural analysis of RNAmer Random90 indicated that this molecule formed stem-loop structures (data not shown), and in the case of the phosphorylated N protein, we observed low-affinity binding with this target compared to viral RNA, suggesting that, in general, N protein did not specifically recognize double-stranded RNA.

Such stem-loop structures have also been identified in the 5′ end of several other coronaviruses, including BCoV DI-RNA (10, 11) and MHV (75), and these sites may therefore also act as high-affinity sites for N protein. However, with that said, in their kinetic analysis, Stohlman et al. (68) located only one high-affinity binding site on the MHV leader RNA that bound MHV N protein, and this site encompassed the MHV core element. But discrepancies between our findings with IBV leader sequence and IBV N protein and the MHV leader sequence and MHV N protein, may be a reflection of the inherent properties of the molecules themselves or of the different kinetic analysis used.

The high-affinity association of phosphorylated N protein with the leader sequence and TAS may have implications for viral translation and possibly replication. If coronavirus mRNAs are translated in a cap-dependent manner, in that they initiate translation at the 5′ end of the leader sequence, then the ribosome may be in conflict with the N protein when it scans along the leader sequence for the translation start codon. However, Tahara et al. (70) have speculated that N protein enhances the translation of MHV mRNAs. In this case, one may hypothesize that by binding to the leader RNA, N protein may reduce the secondary structure to increase the efficiency of translation.

N protein may also bind, with high affinity, to the TAS elements located along the coronavirus genome, and one may therefore speculate that this interaction is involved in the efficiency of transcription of (minus) sgRNAs. Also, N protein may bind to sites that are very similar in sequence to the core element (44) to facilitate transcription at these sites. Although the caveat is that N protein is not required to rescue all of the full-length coronavirus clones so far described, the presence of N protein does increase the rescue efficiency. An alternative is that the TAS sites act as nucleation sites for N protein to facilitate the encapsidation of virus RNAs. Such binding sites may act separately from the packaging signal that promotes a specific interaction with the N protein and the genomic RNA (18, 37) and presumably is required for the efficient packaging of the genomic RNA, but not sgRNAs, into core particles. MHV genomic RNA has been reported to be incorporated into the virion in the absence of N protein (38).

In their review, Laude and Masters (31) described how several workers speculated that phosphorylation of N protein may determine its binding affinity with RNA. Our data indicated that phosphorylation of N protein decreased the affinity of N protein for random RNA. Two possible mechanisms may account for this regulation. Phosphorylation of N protein may alter its conformation and thus affect the RNA binding site(s). Stohlman et al. (69) suggested that phosphorylation of MHV N

protein could lead to substantial conformational changes in protein structure, and phosphorylation of human immunodeficiency virus type 1 Rev protein was shown to alter its conformation and RNA binding properties (21). Our mass spectroscopic data would support the hypothesis of Stohlman et al. (69), in that phosphorylation occurs proximal to RNA binding domains. Alternatively, phosphorylation of N protein could add negative charge to the RNA binding domains and thus reduce electrostatic interaction with target RNA. A similar mechanism has been proposed to regulate binding of potato virus A coat protein to RNA (26). While this would explain the overall slight binding difference between $N_{nonphos}$ and N_{phos} with viral RNA, such an interaction probably does not account for the large difference in binding between N_{phos} protein and random RNA. Although the role of the conserved core sequence in N protein binding has been known for sometime, the mechanism by which this is achieved was not. Our kinetic study would suggest that the core sequence determines the specificity of IBV N protein binding with viral RNA by increasing the association rate. However, this is not the only site within the IBV leader that promotes high-affinity binding with N protein, and the possibly exists that these structures act in concert to promote optimal binding.

ACKNOWLEDGMENTS

This work was supported by a BBSRC project grant (45/S12883) to J.A.H.

We thank Paul Britton for help in design of the leader RNAmers and Dave Cavanagh (IAH Compton) for the generous donation of pCD-61.

REFERENCES

1. **Almazan, F., J. M. Gonzalez, Z. Penzes, A. Izeta, E. Calvo, J. Palana-Duran, and L. Enjuanes.** 2000. Engineering the largest RNA virus genome as an infectious bacterial artificial chromosome. Proc. Natl. Acad. Sci. USA **97:** 5516–5521.
2. **Baric, R. S., G. W. Nelson, J. O. Fleming, R. J. Deans, J. G. Keck, N. Casteel, and S. A. Stohlman.** 1988. Interactions between coronavirus nucleocapsid protein and viral RNAs: implications for viral transcription. J. Virol. **62:** 4280–4287.
3. **Barik, S., and A. K. Banerjee.** 1992. Phosphorylation by cellular casein kinase II is essential for transcriptional activity of vesicular stomatitis virus phosphoprotein P. Proc. Natl. Acad. Sci. USA **89:**6570–6574.
4. **Blaesing, F., C. Weigel, M. Welzeck, and W. Messer.** 2000. Analysis of the DNA-binding domain of Escherichia coli DnaA protein. Mol. Microbiol. **36:**557–569.
5. **Boursnell, M. E. G., M. M. Binns, I. J. Foulds, and T. D. K. Brown.** 1985. Sequence of the nucleocapsid genes from two strains of avian infectious bronchitis virus. J. Gen. Virol. **66:**573–580.
6. **Brian, D. A., and W. J. M. Spaan.** 1997. Recombination and coronavirus defective interfering RNAs. Semin. Virol. **8:**101–111.
7. **Brierley, I., M. E. G. Boursnell, M. M. Binns, B. Bilimoria, V. C. Blok, T. D. K. Brown, and S. C. Inglis.** 1987. An efficient ribosomal frame-shifting signal in the polymerase-encoding region of the coronavirus IBV. EMBO J. **6:**3779–3785.
8. **Casais, R., V. Theil, S. G. Siddell, D. Cavanagh, and P. Britton.** 2001. Reverse genetics system for the avian coronavirus infectious bronchitis virus. J. Virol. **75:**12359–12369.
9. **Cavanagh, D.** 1997. *Nidovirales*: a new order comprising *Coronaviridae* and *Arteriviridae.* Arch. Virol. **142:**629–633.
10. **Chang, R. Y., M. A. Hofmann, P. B. Sethna, and D. A. Brian.** 1994. A *cis*-acting function for the coronavirus leader in defective interfering RNA replication. J. Virol. **68:**8223–8231.
11. **Chang, R. Y., R. Krishnan, and D. A. Brian.** 1996. The UCUAAAC promoter motif is not required for high-frequency leader recombination in bovine coronavirus defective interfering RNA. J. Virol. **70:**2720–2729.
12. **Chen, H., B. Coote, S. Attree, and J. A. Hiscox.** 2003. Evaluation of a nucleoprotein-based enzyme-linked immunosorbent assay for the detection of antibodies against infectious bronchitis virus. Avian Pathol. **32:**519–526.
13. **Chen, H., T. Wurm, P. Britton, G. Brooks, and J. A. Hiscox.** 2002. Interaction of the coronavirus nucleoprotein with nucleolar antigens and the host cell. J. Virol. **76:**5233–5250.
14. **Cologna, R., J. F. Sapgnolo, and B. Hogue.** 2000. Identification of nucleocapsid binding sites within coronavirus-defective genomes. Virology **277:** 235–249.
15. **Dalton, K., R. Casais, K. Shaw, K. Stirrups, S. Evans, P. Britton, T. D. K. Brown, and D. Cavanagh.** 2001. Identification of the *cis*-acting sequences required for coronavirus infectious bronchitis virus defective RNA replication and rescue. J. Virol. **75:**125–133.
16. **Dalton, K., Z. Penzes, C. Wroe, K. Stirrups, S. Evans, K. Shaw, T. D. K. Brown, P. Britton, and D. Cavanagh.** 1998. Sequence elements involved in the rescue of IBV defective RNA CD-91. Adv. Exp. Med. Biol. **440:**253–257.
17. **Davies, H. A., R. R. Dourmashkin, and R. MacNaughton.** 1981. Ribonucleoprotein of avian infectious bronchitis virus. J. Gen. Virol. **53:**67–74.
18. **Escors, D., A. Izeta, C. Capiscol, and L. Enjuanes.** 2003. Transmissible gastroenteritis coronavirus packaging signal is located at the 5′ end of the virus genome. J. Virol. **77:**7890–7902.
19. **Escors, D., J. Ortego, H. Laude, and L. Enjuanes.** 2001. The membrane M protein carboxy terminus binds to transmissible gastroenteritis coronavirus core and contributes to core stability. J. Virol. **75:**1312–1324.
20. **Fosmire, J., K. Hwang, and S. Makino.** 1992. Identification and characterization of a coronavirus packaging signal. J. Virol. **66:**3522–3530.
21. **Fouts, D. E., H. L. True, K. A. Cengel, and D. W. Celander.** 1997. Site-specific phosphorylation of the human immunodeficiency virus type-1 Rev protein accelerates formation of an efficient RNA-binding conformation. Biochemistry **43:**13256–13262.
22. **Hiscox, J. A.** 2002. The nucleolus–a gateway to viral infection? Arch. Virol. **147:**1077–1089.
23. **Hiscox, J. A.** 2003. The interaction of animal cytoplasmic RNA viruses with the nucleus to facilitate replication. Virus Res. **95:**13–22.
24. **Hiscox, J. A., K. L. Mawditt, D. Cavanagh, and P. Britton.** 1995. Investigation of the control of coronavirus subgenomic mRNA transcription by using T7-generated negative-sense RNA transcripts. J. Virol. **69:**6219–6227.
25. **Hiscox, J. A., T. Wurm, L. Wilson, D. Cavanagh, P. Britton, and G. Brooks.** 2001. The coronavirus infectious bronchitis virus nucleoprotein localizes to the nucleolus. J. Virol. **75:**506–512.
26. **Ivanov, K. I., P. Puustinen, A. Mertis, M. Saarma, and K. Makinen.** 2001. Phosphorylation down-regulates the RNA binding function of the coat protein of potato virus A. J. Biol. Chem. **276:**13530–13540.
27. **Katsamba, P. S., S. Park, and I. A. Laird-Offringa.** 2002. Kinetic studies of RNA-protein interactions using surface plasmon resonance. Methods **26:**95–104.
28. **Kortt, A. A., E. Nice, and L. C. Gruen.** 1999. Analysis of the binding of the Fab fragment of monoclonal antibody NC10 to influenza virus N9 neuraminidase from tern and whale using the BIAcore Biosensor: effect of immobilization level and flow rate on kinetic analysis. Anal. Biochem. **273:**133–141.
29. **Krishna, N. K., D. Marshall, and A. Schneemann.** 2003. Analysis of RNA packaging in wild-type and mosaic protein capsids of flock house virus using recombinant baculovirus vectors. Virology **305:**10–24.
30. **Lai, M. M. C., and D. Cavanagh.** 1997. The molecular biology of coronaviruses. Adv. Virus Res. **48:**1–100.
31. **Laude, H., and P. S. Masters.** 1995. The coronavirus nucleocapsid protein, p. 141–163. *In* S. G. Siddell (ed.), The coronaviridae. Plenum Press, New York, N.Y.
32. **Litchfield, D. W.** 2003. Protein kinase CK2: structure, regulation and role in cellular decisions of life and death. Biochem. J. **369:**1–15.
33. **Lu, Q., A. E. Hutchins, C. M. Doyle, J. R. Lundblad, and R. P. Kwok.** 2003. Acetylation of cAMP-responsive element-binding protein (CREB) by CREB-binding protein enhances CREB-dependent transcription. J. Biol. Chem. **278:**15727–15734.
34. **Marra, M. A., S. J. M. Jones, C. R. Astell, et al.** 2003. The genome sequence of the SARS-associated coronavirus. Science **300:**1399–1404.
35. **Masters, P. S.** 1992. Localization of an RNA-binding domain in the nucleocapsid protein of the coronavirus mouse hepatitis virus. Arch. Virol. **125:** 141–160.
36. **Mohandas, D. V., and S. Dales.** 1991. Endosomal association of a protein phosphatase with high dephosphorylating activity against a coronavirus nucleocapsid protein. FEBS Lett. **282:**419–424.
37. **Molenkamp, R., and W. J. M. Spaan.** 1997. Identification of a specific interaction between the coronavirus mouse hepatitis virus A59 nucleocapsid protein and packaging signal. Virology **239:**78–86.
38. **Narayanan, K., C.-J. Chen, J. Maeda, and S. Makino.** 2003. Nucleocapsid-independent specific viral RNA packaging via viral envelope protein and viral RNA signal. J. Virol. **77:**2922–2927.
39. **Narayanan, K., A. Maeda, J. Maeda, and S. Makino.** 2000. Characterization of the coronavirus M protein and nucleocapsid interaction in infected cells. J. Virol. **74:**8127–8134.
40. **Nelson, G. W., and S. A. Stohlman.** 1993. Localization of the RNA-binding domain of mouse hepatitis virus nucleocapsid protein. J. Gen. Virol. **74:** 1975–1979.
41. **Nelson, G. W., S. A. Stohlman, and S. M. Tahara.** 2000. High affinity interaction between nucleocapsid protein and leader/intergenic sequence of mouse hepatitis virus RNA. J. Gen. Virol. **81:**181–188.
42. **Ning, Q., S. Lakatoo, M. F. Liu, W. M. Yang, Z. M. Wang, M. J. Phillips, and**

G. A. Levy. 2003. Induction of prothrombinase fgl2 by the nucleocapsid protein of virulent mouse hepatitis virus is dependent on host hepatic nuclear factor-4 alpha. J. Biol. Chem. **278:**15541–15549.
43. **Ott, M., M. Schnolzer, J. Garnica, W. Fischle, S. Emiliani, H. R. Rackwitz, and E. Verdin.** 1999. Acetylation of the HIV-1 Tat protein by p300 is important for its transcriptional activity. Curr. Biol. **9:**1489–1492.
44. **Ozdarendeli, A., S. Ku, S. Rochat, G. D. Williams, S. D. Senanayake, and D. A. Brian.** 2001. Downstream sequences influence the choice between a naturally occurring noncanonical and closely positioned upstream canonical heptameric fusion motif during bovine coronavirus subgenomic mRNA synthesis. J. Virol. **75:**7362–7374.
45. **Park, S., D. G. Myszka, M. Yu, S. J. Littler, and I. A. Laird-Offringa.** 2000. HuD RNA recognition motifs play distinct roles in the formation of a stable complex with AU-rich RNA. Mol. Cell. Biol. **20:**4765–4772.
46. **Parker, M. M., and P. S. Masters.** 1990. Sequence comparison of the N genes of 5 strains of the coronavirus mouse hepatitis-virus suggests a 3 domain-structure for the nucleocapsid protein. Virology **179:**463–468.
47. **Penzes, Z., C. Wroe, T. D. K. Brown, P. Britton, and D. Cavanagh.** 1996. Replication and packaging of coronavirus infectious bronchitis virus defective RNAs lacking a long open reading frame. J. Virol. **70:**8660–8668.
48. **Risco, C., I. M. Anton, L. Enjuanes, and J. L. Carrascosa.** 1996. The transmissible gastroenteritis coronavirus contains a spherical core shell consisting of M and N proteins. J. Virol. **70:**4773–4777.
49. **Robbins, S. G., M. F. Frana, J. J. McGowan, J. F. Boyle, and K. V. Holmes.** 1986. RNA-binding proteins of MHV: detection of monomeric and multimeric N protein with an RNA overlay protein blot assay. Virology **150:**402–410.
50. **Roepstorff, P., and J. Fohlman.** 1984. Proposal for a common nomenclature for sequence ions in mass spectra of peptides. Biomed. Mass Spectrom. **11:**601.
51. **Rowland, R. R., R. Kerwin, C. Kuckleburg, A. Sperlich, and D. A. Benfield.** 1999. The localisation of porcine reproductive and respiratory syndrome virus nucleocapsid protein to the nucleolus of infected cells and identification of a potential nucleolar localization signal sequence. Virus Res. **64:**1–12.
52. **Rowland, R. R. R., and D. Yoo.** 2003. Nucleolar-cytoplasmic shuttling of PRRSV nucleocapsid protein: a simple case of molecular mimicry or the complex regulation by nuclear import, nucleolar localization and nuclear export signal sequences. Virus Res. **95:**23–33.
53. **Sapats, S. I., F. Ashton, P. J. Wright, and J. Ignjatovic.** 1996. Novel variation in the N protein of avian infectious bronchitis virus. Virology **226:**412–417.
54. **Sawicki, D. L., T. Wang, and S. G. Sawicki.** 2001. The RNA structures engaged in replication and transcription of the A59 strain of mouse hepatitis virus. J. Gen. Virol. **82:**385–396.
55. **Sawicki, S. G., and D. L. Sawicki.** 1986. Coronavirus minus-strand RNA synthesis and effect of cyclohexamide on coronavirus RNA synthesis. J. Virol. **57:**328–334.
56. **Sawicki, S. G., and D. L. Sawicki.** 1990. Coronavirus transcription: subgenomic mouse hepatitis virus replicative intermediates function in RNA synthesis. J. Virol. **64:**1050–1056.
57. **Sawicki, S. G., and D. L. Sawicki.** 1998. A new model for coronavirus transcription. Adv. Exp. Med. Biol. **440:**215–219.
58. **Schneemann, A., T. M. Gallagher, and R. R. Rueckert.** 1994. Reconstitution of flock house provirions: a model system for studying structure and assembly. J. Virol. **68:**4547–4556.
59. **Sethna, P. B., and D. A. Brian.** 1997. Coronavirus genomic and subgenomic minus-strand RNAs copartition in membrane-protected replication complexes. J. Virol. **71:**7744–7749.
60. **Sethna, P. B., S.-L. Hung, and D. A. Brian.** 1991. Minus-strand copies of replicating coronavirus mRNAs contain anti-leaders. J. Virol. **65:**320–325.
61. **Sevier, C. S., and C. A. Kaiser.** 2002. Formation and transfer of disulphide bonds in living cells. Nat. Rev. Mol. Cell Biol. **3:**836–847.
62. **Shiell, B. J., D. R. Gardner, G. Crameri, B. T. Eaton, and W. P. Michalski.** 2003. Sites of phosphorylation of P and V proteins from Hendra and Nipah viruses: newly emerged members of Paramyxoviridae. Virus Res. **92:**55–65.
63. **Siddell, S. G. (ed.).** 1995. The coronaviridae. Plenum Press, New York, N.Y.
64. **Siddell, S. G., A. Barthel, and V. Termeulen.** 1981. Coronavirus JHM: a virion-associated protein kinase. J. Gen. Virol. **52:**235–243.
65. **Stirrups, K., K. Shaw, S. Evans, K. Dalton, R. Casais, D. Cavanagh, and P. Britton.** 2000. Expression of reporter genes from the coronavirus infectious bronchitis virus defective RNA CD-61. J. Gen. Virol. **81:**1687–1698.
66. **Stirrups, K., K. Shaw, S. Evans, K. Dalton, D. Cavanagh, and P. Britton.** 2000. Leader switching occurs during the rescue of defective RNAs by heterologous strains of the coronavirus infectious bronchitis virus. J. Gen. Virol. **81:**791–801.
67. **Stockley, P. G., A. J. Baron, C. M. Wild, I. D. Parsons, C. M. Miller, C. A. Holtham, and S. Baumberg.** 1998. Dissecting the molecular details of prokaryotic transcriptional control by surface plasmon resonance: the methionine and arginine repressor proteins. Biosens. Bioelectron. **13:**637–650.
68. **Stohlman, S. A., R. S. Baric, G. N. Nelson, L. H. Soe, L. M. Welter, and R. J. Deans.** 1988. Specific interaction between coronavirus leader RNA and nucleocapsid protein. J. Virol. **62:**4288–4295.
69. **Stohlman, S. A., J. O. Fleming, C. D. Patton, and M. M. C. Lai.** 1983. Synthesis and subcellular-localization of the murine coronavirus nucleocapsid protein. Virology **130:**527–532.
70. **Tahara, S. M., T. A. Dietlin, C. C. Bergmann, G. W. Nelson, S. Kyuwa, R. P. Anthony, and S. A. Stohlman.** 1994. Coronavirus translational regulation: leader affects mRNA efficiency. Virology **202:**621–630.
71. **Thiel, V., J. Herold, B. Schelle, and S. G. Siddell.** 2001. Infectious RNA transcribed *in vitro* from a cDNA copy of the human coronavirus genome cloned in vaccinia virus. J. Gen. Virol. **82:**1273–1281.
72. **Thiel, V., J. Herold, B. Schelle, and S. G. Siddell.** 2001. Viral replicase gene products suffice for coronavirus discontinuous transcription. J. Virol. **75:**6676–6681.
73. **Tihova, M., K. A. Dryden, T. V. Le, S. C. Harvey, J. E. Johnson, M. Yeager, and A. Schneemann.** 2004. Nodavirus coat protein imposes dodecahedral RNA structure independent of nucleotide sequence and length. J. Virol. **78:**2897–2905.
74. **Tijms, M. A., Y. van der Meer, and E. J. Snijder.** 2002. Nuclear localization of nonstructural protein 1 and nucleocapsid protein of equine arteritis virus. J. Gen. Virol. **83:**795–800.
75. **Wang, Y., and X. Zhang.** 2000. The leader RNA of coronavirus mouse hepatitis virus contains an enhancer-like element for subgenomic mRNA transcription. J. Virol. **74:**10571–10580.
76. **Waysbort, A., S. Bonnal, S. Audigier, J.-P. Esteve, and A.-C. Prats.** 2001. Pyrimidine tract binding protein and La autoantigen interact differently with the 5′ untranslated regions of lentivirus and oncoretrovirus mRNAs. FEBS Lett. **490:**54–58.
77. **Weidman, M. K., R. Sharma, S. Raychaudhuri, P. Kundu, W. Tsai, and A. Dasgupta.** 2003. The interaction of cytoplasmic RNA viruses with the nucleus. Virus Res. **95:**75–85.
78. **White, E. K., T. Moore-Jarrett, and H. E. Ruley.** 2001. PUM2, a novel murine Puf protein, and its consensus RNA-binding site. RNA **7:**1855–1866.
79. **Wilbur, S. M., G. W. Nelson, M. M. C. Lai, M. McMillan, and S. A. Stohlman.** 1986. Phosphorylation of the mouse hepatitis virus nucleocapsid protein. Biochem. Biophys. Res. Commun. **141:**7–12.
80. **Wootton, S. K., R. R. R. Rowland, and D. Yoo.** 2002. Phosphorylation of the porcine reproductive and respiratory syndrome virus nucleocapsid protein. J. Virol. **76:**10569–10576.
81. **Wurm, T., H. Chen, P. Britton, G. Brooks, and J. A. Hiscox.** 2001. Localization to the nucleolus is a common feature of coronavirus nucleoproteins and the protein may disrupt host cell division. J. Virol. **75:**9345–9356.
82. **Yount, B., K. M. Curtis, and R. S. Baric.** 2000. Strategy for systematic assembly of large RNA and DNA genomes: transmissible gastroenteritis virus model. J. Virol. **74:**10600–10611.
83. **Yount, B., K. M. Curtis, E. A. Fritz, L. E. Hensley, P. B. Jahrling, E. Prentice, M. R. Denison, T. W. Geisbert, and R. S. Baric.** 2003. Reverse genetics with a full-length infectious cDNA of severe acute respiratory syndrome coronavirus. Proc. Natl. Acad. Sci. USA **100:**12995–13000.
84. **Zhou, M. L., A. K. Williams, S. I. Chung, L. Wang, and E. W. Collisson.** 1996. Infectious bronchitis virus nucleocapsid protein binds RNA sequences in the 3′ terminus of the genome. Virology **217:**191–199.